International Journal of Geo-Information

MDPI

Article

A Pilot Study on a GPU-Accelerated Voxel Simulation Framework for 3D Indoor and Urban-Scale Gas Dispersion and Aerosol Transport

Haowen Xu [1], Sisi Zlatanova [1,*], Ben Gorte [1], Rabindra Lamsal [1], David Heslop [2], Ruiyu Liang [3] and Ismet Canbulat [3]

[1] Geospatial Research Innovations and Development (GRID), School of Built Environment, UNSW Sydney, Sydney, NSW 2052, Australia; haowen.xu.phd@gmail.com (H.X.)
[2] School of Population Health, UNSW Sydney, Sydney, NSW 2052, Australia
[3] School of Minerals and Energy Resources Engineering, UNSW Sydney, Sydney, NSW 2052, Australia
* Correspondence: s.zlatanova@unsw.edu.au

Abstract

The increasing complexity of environmental analysis requires new approaches for interactive-scale simulation across indoor and urban spaces. While computational fluid dynamics (CFD) models provide detailed representations of gas dispersion and aerosol transport, they are often computationally intensive for interactive environmental analysis and integration into digital twin platforms. This pilot study presents a GPU-accelerated voxel simulation framework for modeling three-dimensional gas dispersion and aerosol transport using structured voxel representations derived from BIM, LiDAR, GIS, and other 3D built-environment datasets. The framework provides physically informed, CFD-inspired simulation at sub-meter to meter-scale spatial resolutions while maintaining interactive runtime performance suitable for building management, ventilation analysis, environmental monitoring, hazard assessment, and emergency response applications. Transport dynamics are modeled using a discretized advection–diffusion formulation incorporating airflow-driven advection, diffusion, source emissions, and voxel-level sink mechanisms. A key contribution is the development of a voxel-native GPU-parallel computational architecture implemented in Python 3.10.20 using Taichi kernels. Prototype simulations and comparative validation against a benchmark ANSYS Fluent 20.1 simulation demonstrate stable transport behavior, encouraging agreement with the CFD solution, browser-based three-dimensional visualization, and efficient execution on commodity GPU hardware. Experimental scenarios include a voxelized three-story Industry Foundation Classes (IFC) building model comprising approximately 34.5 million active voxels (582 × 382 × 155 voxels) and an urban-scale 3D city model spanning approximately 300 × 300 × 150 m and containing up to 13.9 million active voxels. Simulations containing tens of millions of voxels were completed within minutes on a single consumer-grade GPU, demonstrating the scalability of the framework. These results demonstrate that the proposed framework provides an efficient voxel-based approximation of gas dispersion suitable for interactive environmental analysis and can support future integration with digital twin and AI-assisted environmental simulation systems.

Keywords: voxel-based simulation; gas dispersion; aerosol transport; 3D indoor digital twins; parallel computing

Check for updates

Academic Editors: Wolfgang Kainz, Chaowei Yang, Daniel Q. Duffy, Xiao Huang and Lingbo Liu

Received: 10 June 2026
Revised: 22 August 2026
Accepted: 26 August 2026
Published: 5 September 2026

Copyright: © 2026 by the authors. Published by MDPI on behalf of the International Society for Photogrammetry and Remote Sensing. Licensee MDPI, Basel, Switzerland. This article is an open access article distributed under the terms and conditions of the Creative Commons Attribution (CC BY) license.

1. Introduction

Indoor environmental hazards, including toxic gas leakage, aerosolized pollutants, smoke propagation, and airborne contaminant transport, pose significant risks to human health, building safety, and emergency response operations in residential, commercial, and industrial environments [1,2]. The increasing availability of voxelization tools and voxelized indoor environments derived from Building Information Modeling (BIM), LiDAR, other scanning technologies, and digital twin platforms has created new opportunities for near-real-time 3D environmental hazard simulation within built spaces [3]. Recent incidents involving industrial gas leakage, indoor smoke exposure during structural fires, and concerns regarding airborne disease transmission have further highlighted the importance of understanding contaminant transport dynamics in complex indoor environments [4–6]. Physically informed and computationally efficient simulation of indoor gas dispersion and aerosol transport can support a wide range of applications, including building ventilation design and assessment, building retrofit and resilience planning, emergency evacuation analysis, hazardous material management, indoor air quality assessment, and AI-assisted digital twin systems for smart building and infrastructure management [7–10].

Existing approaches for simulating indoor gas dispersion and aerosol transport are largely dominated by Computational Fluid Dynamics (CFD)-based methods, which model fluid flow and contaminant transport using numerical formulations derived from the Navier–Stokes equations and advection–diffusion transport equations [11,12]. Widely used CFD platforms, including ANSYS Fluent, OpenFOAM, and Fire Dynamics Simulator (FDS), have been extensively applied for simulating airflow dynamics, smoke propagation, ventilation performance, thermal transport, and airborne contaminant dispersion in indoor environments [13–15]. These models are capable of representing complex fluid behaviors, including turbulence, buoyancy-driven flow, heat transfer, multi-species transport, and interactions between airflow and building geometries [11,12]. In addition, PDE-based environmental transport models have been widely adopted in studies related to indoor air quality assessment, hazardous gas leakage analysis, industrial safety evaluation, and airborne disease transmission [7,16]. Such approaches provide physically grounded and high-fidelity representations of contaminant transport processes and have become important tools for building design, ventilation optimization, fire safety engineering, environmental assessment, and emergency response analysis in complex indoor environments [17,18].

Despite their strong physical foundations and high-fidelity modeling capabilities, many existing CFD-based simulation frameworks face practical limitations when applied to emerging digital twin and AI-assisted environmental simulation applications [19–21]. Traditional CFD workflows often rely on complex mesh-based preprocessing pipelines, including geometry cleaning, mesh generation, boundary condition specification, and solver configuration, which can be difficult to scale for large numbers of buildings and indoor environments increasingly represented through voxelized BIM, LiDAR, and digital twin datasets [12,22]. In addition, many legacy simulation platforms were originally designed as standalone engineering tools and provide limited support for cloud-native deployment, online simulation services, programmable APIs, and accessible user workflows, reducing their compatibility with dynamically updated digital twins, and broader use by non-expert stakeholders [8,19,23]. The computational cost and runtime requirements of high-fidelity CFD simulations can also limit interactivity, rapid scenario exploration, and near-real-time operational decision support [11,12]. Furthermore, limited interoperability with AI agent pipelines, LLM-enabled orchestration systems, and immersive visualization platforms, including web-based digital twins, augmented reality (AR), and mixed-reality environments, often requires substantial additional integration effort [24]. These challenges motivate the development of lightweight, programmable, and AI-native environmental simulation

frameworks capable of supporting interactive, scalable, and digitally integrated hazard simulation workflows.

This paper presents an early-stage exploration of a GPU-accelerated, voxel-based simulation framework for three-dimensional indoor and urban-scale gas dispersion and aerosol transport within structured voxel environments. Rather than replacing conventional CFD solvers, the proposed framework explores a modular computational architecture that integrates voxel-based contaminant transport with parameterized or externally supplied airflow fields, including those generated by established CFD software. Developed in Python, the framework combines a GPU-parallel advection–diffusion solver, configurable source and sink formulations, species-dependent transport parameters, and structured voxel representations within a unified computational environment. To demonstrate the feasibility of the proposed framework, four representative indoor, urban, and building-scale case studies are presented, together with an initial quantitative validation against an ANSYS Fluent benchmark using identical geometry, source conditions, ventilation configuration, and prescribed airflow fields. The results demonstrate encouraging agreement in plume morphology while illustrating the practical computational performance of the GPU-parallel implementation across domains ranging from residential buildings to urban-scale environments containing more than 34 million active voxels on consumer-grade GPU hardware. Although the current work represents an initial proof-of-concept rather than a fully validated predictive environmental simulation system, it establishes a modular computational foundation for the future integration of CFD-derived airflow fields, AI surrogate models, and sensor-informed digital twins for large-scale environmental simulation.

The remainder of this paper is organized as follows. Section 2 introduces the conceptual framework, system architecture, and mathematical formulation of the proposed voxel-based environmental simulation framework. Section 3 presents the modular airflow modeling approach, contaminant transport formulation, GPU-parallel stencil-based implementation, and numerical stability considerations. Section 4 demonstrates the framework through four representative indoor, urban, and building-scale simulation scenarios, followed by quantitative validation against an ANSYS Fluent benchmark, scenario configuration and reproducibility summaries, and a computational performance evaluation. Finally, Section 5 concludes the paper with a discussion of the current limitations, future research directions, and opportunities for integrating the proposed framework with digital twins, immersive visualization systems, and AI-assisted environmental simulation.

2. Literature Review

This section first reviews the physical processes and theoretical foundations and computational approaches for indoor gas dispersion and aerosol transport simulation, followed by widely used commercial and open-source simulation platforms. Finally, we discuss current research gaps related to voxel-native simulation, digital twin interoperability, interactive computation, and AI-agent integration that motivate the proposed framework.

2.1. Physical Processes and Computational Approaches

Indoor aerosol and gas transport simulations commonly incorporate several physical transport processes, which are reviewed here at a high level. Advection describes the movement of contaminants driven by surrounding airflow fields, while turbulent diffusion represents the spreading and mixing of contaminants caused by turbulent air motion [25]. Buoyancy-driven transport accounts for density differences and thermal effects that can cause gases or aerosols to rise or sink within indoor environments, making species density and release conditions important considerations when modeling hazardous gas dispersion [26,27]. Particle settling represents gravitational sedimentation of aerosols toward

surfaces, whereas deposition describes the accumulation of particles on walls, floors, ceilings, or other objects [28]. Ventilation exchange models the removal and introduction of contaminants through HVAC systems, windows, or airflow openings, while source and sink mechanisms represent contaminant emission, filtration, chemical decay, or other removal processes [29,30]. Depending on the simulation objective, contaminants may be modeled either as passive scalar concentration fields or as discrete particles interacting with surrounding airflow fields [31,32].

Existing computational approaches for modeling indoor airflow, contaminant transport, smoke propagation, and airborne particle dispersion are commonly based on CFD methods derived from governing partial differential equations (PDEs), and are scientifically mature with strong theoretical foundations for indoor environmental simulation [12,33]. These approaches typically solve the Navier–Stokes equations together with advection–diffusion transport equations to represent airflow dynamics and contaminant concentration evolution over time and space [33,34]. Common computational methods include Reynolds-Averaged Navier–Stokes (RANS) models, Large Eddy Simulation (LES), passive scalar transport models, and Eulerian–Lagrangian particle tracking approaches [12,31,32]. RANS-based methods are widely adopted for practical indoor airflow simulations due to their relatively lower computational requirements, while LES approaches can provide higher-fidelity representations of transient turbulent flow structures at substantially higher computational cost [11,12,32]. Collectively, these computational approaches form the theoretical foundation of many existing indoor environmental simulation tools and commercial CFD platforms used for airflow analysis, smoke propagation modeling, ventilation assessment, and airborne contaminant transport simulation. The next subsection reviews several widely adopted simulation tools and platforms developed based on these computational principles [11,12,35].

2.2. Indoor Gas Simulation Software Platforms

A wide range of commercial and open-source CFD software platforms have been developed for indoor airflow, gas dispersion, smoke propagation, and aerosol transport simulation. Widely adopted platforms include ANSYS Fluent, OpenFOAM, Fire Dynamics Simulator (FDS), COMSOL Multiphysics, and STAR-CCM+, which are commonly used for airflow analysis, ventilation assessment, thermal transport simulation, smoke propagation modeling, and airborne contaminant transport studies within indoor environments [12,15,35]. These platforms are typically implemented using numerical CFD approaches based on finite volume, finite element, or finite difference methods to solve the Navier–Stokes equations together with advection–diffusion transport formulations across discretized computational domains [34–36]. Many systems further support RANS, LES, passive scalar transport, Eulerian–Lagrangian particle tracking, thermal buoyancy modeling, and multi-species contaminant simulation for complex indoor geometries and ventilation configurations [31,35]. Such platforms have been extensively applied in building ventilation design, fire safety engineering, industrial hazard assessment, indoor air quality analysis, and airborne disease transmission studies [7,12,35]. In recent years, several studies have also explored coupling CFD-based airflow simulation with sensor networks, digital twins, and interactive-scale environmental monitoring systems for intelligent building management applications [8,19]. These developments create opportunities for coupling gas dispersion and aerosol transport models with large-scale, multi-domain urban digital twins, enabling broader urban operations and management applications through human-in-the-loop decision support, interactive-scale, environmental monitoring, and cross-domain simulation integration [37–39].

2.3. Research Gaps and Motivation

Despite their strong physical foundations and high-fidelity modeling capabilities, many existing CFD-based simulation platforms face practical limitations when applied to emerging digital twin and AI-assisted environmental simulation applications. Several important challenges can be identified:

- Mesh dependency and preprocessing complexity:Traditional CFD workflows often rely on geometry reconstruction, mesh generation, boundary condition specification, and solver configuration, which can become difficult to scale for large numbers of buildings and indoor environments increasingly represented through voxelized BIM, LiDAR, and digital twin datasets [12,35].
- Computational scalability limitations: High-fidelity CFD simulations are often computationally expensive and are commonly applied to relatively small room-scale or building-scale environments due to runtime and hardware constraints. Scaling such simulations toward larger multi-building, campus-scale, or city-scale digital twin environments can become challenging, particularly for repeated simulations and operational workflows [11,12].
- Limited support for cloud-native and AI-integrated workflows: Many existing simulation platforms were originally developed as standalone engineering tools with limited support for cloud-native deployment, web-based simulation services, programmable APIs, and integration with digital twin platforms. These limitations can hinder their incorporation into dynamically updated building and urban management systems that require automated data exchange and interactive-scale simulation capabilities [8,19].
- Limited interactivity and interactive-scale simulation capability: The runtime requirements of high-fidelity CFD simulations can limit rapid scenario exploration, operational decision support, and near-real-time environmental analysis, particularly for applications requiring repeated simulations or interactive workflows [11,12].
- Challenges in immersive visualization integration: Integrating conventional CFD workflows with immersive visualization systems, web-based digital twins, and emerging AR/MR environments often requires substantial additional processing and custom engineering effort [40].

These challenges motivate the development of lightweight, programmable, and voxel-compatible environmental simulation frameworks capable of leveraging the increasing availability of BIM, LiDAR, and 3D city model datasets that can be readily transformed into voxel-based representations for environmental simulation [41,42]. Such frameworks can support interactive-scale computation for building-, campus-, and city-scale 3D simulations, while enabling digital twin interoperability and agentic AI-native environmental simulation workflows [24,43]. Rather than replacing traditional high-fidelity CFD systems, the proposed framework is intended to complement existing approaches by enabling practical operational analysis, rapid hazard assessment, ventilation scenario exploration, and intelligent urban and building management under realistic computational and time constraints.

3. Methodology

This section outlines the study's motivation and core design requirements for interactive-scale indoor gas dispersion and aerosol transport simulation within voxelized environments. We then present the framework architecture, including voxel representation, transport formulations, airflow modeling, and species transport mechanisms. Finally, we describe the GPU-parallel implementation and modular Python-based system design for supporting practical runtime performance, digital twin interoperability, and agentic AI-native simulation workflows.

3.1. Design Requirements

This study aims to develop a lightweight GPU-accelerated voxel simulation framework for modeling indoor gas dispersion, aerosol transport, and smoke propagation within complex built environments. The framework adopts a parameterized transport formulation that allows different gaseous and particulate contaminants to be represented through configurable physical properties and transport parameters, enabling flexible simulation of multiple contaminant species under varying indoor environmental conditions. The framework is intended to support applications including indoor air quality assessment, hazardous gas leakage analysis, ventilation evaluation, emergency response planning, and AI-assisted environmental digital twin systems for smart buildings and infrastructure management. Target users include researchers, building operators, emergency responders, urban digital twin developers, and future agentic AI systems and their AI agents that require the use of interactive-scale environmental simulation capabilities. These use cases define the core design requirements of the proposed simulation framework, summarized as follows:

- Interactive-Scale Environmental Simulation: The framework should support practical operational analysis and interactive-scale environmental simulation across indoor, building-, and potentially larger urban-scale environments under realistic runtime and computational constraints, rather than targeting centimeter-scale engineering precision or long-duration supercomputing-based simulations.
- Support for Large-Scale 3D Built Environments: The system should support structured 3D representations derived from BIM, LiDAR, and digital twin datasets to enable scalable environmental simulation across indoor and urban environments.
- Parameterized Multi-Species Simulation: The framework should support configurable physical properties and transport parameters for simulating different gaseous contaminants, aerosol particles, and smoke species under varying indoor environmental conditions. This parameterization is intended to support future investigation of hazardous gases with different density, diffusivity, and buoyancy characteristics, including rapidly dispersing toxic species.
- GPU-Accelerated Computation: The simulator should leverage GPU-parallel computing and structured voxel connectivity to support computationally efficient indoor airflow and contaminant transport simulation.
- Modular and Programmable Architecture: The framework should adopt a modular Python-based architecture that supports reusable components, extensibility, and integration with external computational workflows.
- Digital Twin and AI-Agent Interoperability: The system should support integration with web platforms, near-real-time sensor systems, immersive visualization environments, digital twins, and emerging AI-agent pipelines through programmable interfaces and interoperable data structures.

Based on these design requirements, we developed a modular Python-based framework that combines GPU-accelerated parallel computing with voxel-based environmental representations to enable scalable simulation of indoor gas dispersion and aerosol transport. The framework is designed to complement traditional CFD models by supporting efficient environmental simulation within emerging digital twin and urban management applications.

3.2. Overall Framework Architecture

We developed a voxel-based environmental simulation framework for modeling indoor gas dispersion and aerosol transport through inter-voxel contaminant transport processes within structured 3D indoor environments. The framework leverages structured voxel connectivity and stencil-based computational schemes to encode physically

informed mass transfer processes across neighboring voxel cells, enabling efficient simulation of contaminant propagation, diffusion, and airflow-driven transport within voxelized indoor spaces. By combining simplified transport formulations with GPU-parallel computation, the system supports interactive-scale simulation of gaseous and aerosol contaminant propagation under varying airflow and ventilation conditions. Rather than targeting ultra-high-fidelity engineering CFD analysis, the framework focuses on practical operational simulation within voxelized indoor environments derived from BIM, LiDAR, and digital twin datasets. Figure 1 illustrates the overall system architecture, which consists of four primary components: (T1) Voxel Environment Representation, (T2) Airflow Modeling, (T3) Gas and Aerosol Transport Simulation, and (T4) Simulation Visualization for Digital Twinning.

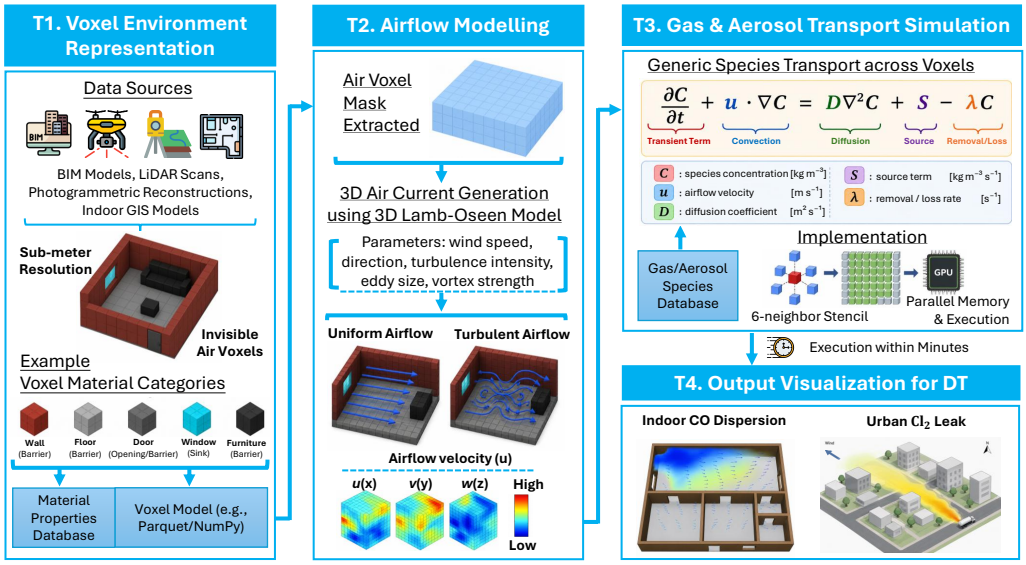


Figure 1. Overview of the proposed GPU-accelerated voxel-based environmental simulation framework for indoor gas dispersion and aerosol transport. The framework integrates voxelized environment representation, parameterized airflow modeling, stencil-based contaminant transport simulation, GPU-parallel computation, and interoperable visualization workflows for indoor and urban-scale environmental analysis.

3.2.1. Voxel Environment Representation

The proposed framework adopts a semantically-rich voxel-based representation for modeling indoor environments and contaminant transport processes. The system is designed to support indoor representations derived from BIM, LiDAR point clouds, 3D GIS models, rasterized occupancy grids, and voxelized digital twin datasets. Input voxel environments may be represented using commonly adopted data formats including CSV, NumPy arrays, Parquet datasets, or other structured tabular or array-based voxel representations. To support indoor environmental simulation, voxels hold information about different semantic categories representing both transport barriers and transportable spaces. Barrier voxels include walls, floors, ceilings, closed door, closed windows, furniture, and other solid indoor structures that restrict contaminant transport and airflow propagation. Transportable voxels primarily represent indoor air volumes through which gaseous and aerosol contaminants may propagate as well as open doors and windows. Additional voxel attributes may also be assigned to represent environmental properties including ventilation openings, material-specific deposition behavior, and localized transport conditions.

The framework further supports configurable source and sink attributes for individual voxels to simulate contaminant emission, ventilation exchange, filtration, chemical decay, or other material addition and removal processes. This parameterized representation en-

ables flexible simulation of different gaseous contaminants, aerosol particles, and smoke species under varying environmental conditions. Following preprocessing and voxel classification, the structured voxel environment is stored using columnar Parquet-based datasets to support efficient storage, scalable loading, and high-performance data management for large indoor environmental simulations.

3.2.2. Airflow Modeling

Airflow is the primary driver of contaminant advection in indoor and urban environments. In conventional CFD, airflow fields are obtained by solving the Navier–Stokes equations together with turbulence-closure models, such as Reynolds–Averaged Navier–Stokes (RANS) or Large Eddy Simulation (LES), to resolve or approximate turbulent flow structures. While these approaches provide high-fidelity airflow predictions, they are computationally demanding and are primarily intended for engineering analysis. Meanwhile, the increasing availability of voxelized building and city models derived from BIM, LiDAR, and 3D GIS has created a growing need for computational frameworks that can readily integrate airflow fields generated by established CFD methods with voxel-based environmental simulations and digital twins.

The proposed framework does not aim to replace CFD solvers or introduce a new turbulence-closure model. Instead, it provides a modular airflow interface that enables voxel-aligned velocity fields to be incorporated from multiple sources, including CFD simulations, AI surrogate models, urban wind datasets, and parameterized airflow generators. Beyond coupling existing airflow models with voxel-based contaminant transport, the framework also provides a voxel-native computational platform for exploring lightweight airflow generation methods that are computationally suitable for large-scale building and urban environmental simulations. These include steady-state or transient CFD simulations, AI surrogate models, externally generated urban wind datasets, and lightweight parameterized airflow generators. By mapping these airflow fields onto structured voxel environments, the framework enables existing CFD capabilities and emerging airflow prediction methods to be readily coupled with voxel-based contaminant transport simulation across the increasing number of building and city models represented as structured voxels.

For applications where high-fidelity airflow fields are unavailable or computationally impractical, the framework also provides several parameterized airflow generators for rapid scenario exploration. These include uniform airflow fields, turbulent uniform airflow, Lamb–Oseen-inspired vortex fields, and turbulent vortex models. Rather than reproducing the turbulence fidelity of RANS or LES, these parameterized models generate representative airflow patterns suitable for exploratory environmental analysis while maintaining computational efficiency. Owing to its modular design, the framework can readily incorporate externally generated airflow fields, including CFD simulations, AI surrogate models, and urban-scale wind products (e.g., building-resolving or city-scale wind datasets) derived from resources such as Feilian-3D, UrbanTALES, and WRF [44,45]. This enables airflow information generated by specialized atmospheric and urban climate models to be directly coupled with the voxel-based contaminant transport simulation.

$$\mathbf{r}_{\perp} = (\mathbf{x} - \mathbf{x}_0) - [(\mathbf{x} - \mathbf{x}_0) \cdot \hat{\mathbf{a}}]\hat{\mathbf{a}}, \qquad r_{\perp} = \|\mathbf{r}_{\perp}\|. \tag{1}$$

After voxel segmentation and indoor environment preprocessing, indoor air voxels are identified and grouped into connected air components using voxel connectivity analysis. Airflow fields are then either generated using the built-in parameterized airflow models or imported from external sources and mapped onto the voxel domain as velocity components in the u, v, and w directions. As an example, the Lamb–Oseen-inspired vortex

model (Equation (1)) generates localized rotational airflow structures that approximate recirculation zones commonly observed near obstacles and ventilation outlets. Here, $\mathbf{x}$ denotes the voxel location, $\mathbf{x}_0$ is the vortex center, $\hat{\mathbf{a}}$ defines the vortex axis, and $r_\perp$ is the radial distance from the voxel to the vortex axis. The circulation strength Γ controls the vortex intensity, while ν governs the diffusion of vorticity. The resulting voxel-aligned velocity fields subsequently drive the advection and transport of gaseous contaminants within the voxel-based advection–diffusion framework.

The Lamb–Oseen-inspired airflow model presented in this study is provided only as one example of the modular airflow generation capability of the proposed framework and should not be interpreted as the universal airflow model for all simulation scenarios. The primary contribution of this work is not the development of a dedicated indoor or outdoor wind model, but rather a voxel-based three-dimensional simulation framework that supports the generation, integration, and coupling of airflow fields with contaminant transport simulations. Airflow fields may be generated using lightweight voxel-based parameterized models, such as the Lamb–Oseen-inspired vortex formulation, or imported from external sources including CFD simulations, AI surrogate models, atmospheric models, and urban-scale wind datasets. Consequently, the framework can be readily adapted to a wide range of application domains, including indoor environments, outdoor urban areas, and underground mines, by replacing the airflow generation module and corresponding transport formulations while maintaining a common voxel-based computational architecture.

3.2.3. Gas and Aerosol Transport Simulation

The proposed framework models indoor gas dispersion and aerosol transport using a voxel-based advection–diffusion transport formulation implemented through stencil-based inter-voxel computation. Contaminant transport is simulated across structured voxel connectivity using localized mass transfer updates between neighboring air voxels. The current implementation adopts a physically informed transport formulation inspired by classical advection–diffusion equations while maintaining computational simplicity suitable for interactive-scale environmental simulation (as shown in Equation (2)).

$$\frac{\partial C}{\partial t} + \mathbf{u} \cdot \nabla C = D\nabla^2 C + S - \lambda C \tag{2}$$

In Equation (2), C represents contaminant concentration within the voxelized indoor environment, while $\mathbf{u} = (u, v, w)$ denotes the airflow velocity field in the three spatial directions. The advection term $\mathbf{u} \cdot \nabla C$ represents airflow-driven contaminant transport and is numerically implemented using a first-order upwind advection scheme within the current prototype. The parameter D represents the diffusion coefficient controlling contaminant mixing and spreading behavior, while the diffusion term $D\nabla^2 C$ is approximated using a structured six-neighbor Laplacian stencil across adjacent voxel cells. The source term S represents contaminant emission processes such as gas leakage, smoke generation, or aerosol release within selected indoor voxels. The sink term λC represents combined contaminant removal processes including ventilation exchange, deposition, filtration, and first-order reaction or decay mechanisms. For aerosol species, the framework additionally incorporates gravity-driven settling behavior through vertical settling velocity adjustments within the airflow transport computation. Collectively, these transport processes enable physically informed simulation of gaseous and aerosol contaminant propagation within structured voxelized indoor environments.

For each contaminant species, the framework computes airflow-driven advection, turbulent diffusion, source emission, and sink removal processes at every simulation timestep.

Advection processes are driven using voxel-aligned airflow velocity fields represented by the u, v, and w velocity components, while diffusion is modeled using a structured six-neighbor Laplacian stencil across adjacent voxel cells. The current prototype adopts a first-order upwind advection scheme together with explicit time integration for concentration updates across the voxel grid. To maintain stable indoor boundary behavior, no-flux wall boundary conditions are approximated by preventing contaminant transport through solid voxels. The framework additionally incorporates configurable physical processes commonly associated with indoor aerosol and gas transport, including aerosol settling, ventilation removal, deposition, filtration, and first-order reaction or decay mechanisms.

Boundary conditions. The proposed framework supports several boundary-condition types through voxel material classifications. Solid walls are treated as impermeable boundaries, where no contaminant flux is exchanged across the wall interface except for optional deposition represented by a first-order sink term. Ventilation openings and exhaust outlets are modeled using prescribed removal coefficients, which remove contaminant mass from the transported scalar field according to the governing source/sink formulation. Open computational boundaries employ prescribed airflow velocity fields supplied by the selected airflow model or imported CFD data, while contaminant transport across these boundaries follows the local advection–diffusion update. Stairwells, corridors, and other connected indoor spaces are represented implicitly through continuous air-voxel connectivity within the structured voxel lattice.

The framework further incorporates a file-based contaminant species knowledge base that stores configurable physical properties and transport parameters for different gaseous and particulate contaminants, including species such as CO, CO_2, SO_2, SF_6, and $PM_{2.5}$. Each contaminant species is represented using parameterized attributes including contaminant type, diffusion coefficient, settling velocity, relative density, reaction or decay coefficients, ventilation removal rates, particle density, particle diameter, and material-dependent deposition velocities. For aerosol species, deposition parameters may additionally be coupled with indoor material categories such as walls, floors, ceilings, furniture, and other obstacle classes to simulate surface accumulation behavior. The framework further incorporates an indoor surface material knowledge base that stores configurable attributes for different obstacle and surface categories, enabling characterization of their material-dependent deposition and contaminant sink behaviors for aerosol species. This configurable species and voxel materials representation enables flexible simulation of different contaminant transport behaviors while supporting future extension toward additional gaseous, particulate, or chemically reactive contaminants.

3.2.4. Output Visualization for Digital Twinning

The framework incorporates a web-based 3D visualization portal developed using vtk.js for interactive visualization of voxelized indoor environments and time-series contaminant transport simulation results. The visualization system supports rendering of indoor room geometries, airflow conditions, and dynamic gas dispersion or aerosol propagation processes across structured voxel grids. Airflow direction and velocity at different spatial locations are visualized using blue vector arrows, enabling users to intuitively inspect indoor ventilation patterns and air circulation behavior. Simulated gas concentrations are represented using a color-mapped volumetric visualization scheme, where different colors indicate varying contaminant concentration levels, allowing rapid identification of high-risk accumulation zones and contaminant transport pathways.

Simulation outputs can be visualized as temporal concentration distributions within indoor spaces, enabling interactive exploration of contaminant propagation patterns, ventilation effects, and localized accumulation behavior under different environmental conditions.

The current prototype exports simulation results using CSV-based outputs containing voxel-level concentration values, spatial coordinates, contaminant species information, and temporal simulation states. These outputs are designed to support interoperability with external visualization and simulation platforms, including 3D game engines such as Unity and Unreal Engine.

Through these interoperable outputs, the framework can support future immersive visualization workflows including extended reality (XR), augmented reality (AR), mixed-reality environments, holographic visualization systems, and interactive digital twin applications for environmental analysis, emergency planning, and intelligent building management.

3.2.5. GPU-Parallel Stencil-Based Computation

The proposed framework adopts a voxel-centric GPU-parallel computational architecture for scalable contaminant transport simulation on structured voxel grids. Rather than relying on irregular mesh traversal or graph-based neighborhood searches, the framework employs a six-neighbor finite-difference stencil to approximate the governing three-dimensional advection–diffusion equation. By exploiting the regular connectivity of structured voxels, localized transport processes can be evaluated efficiently using only adjacent neighboring cells, making the method well suited for massively parallel GPU execution.

The contaminant transport model is discretized on a structured Cartesian voxel lattice. At each simulation time step, the concentration of every voxel is updated using information from its six face-connected neighbors corresponding to the positive and negative directions of the three spatial axes. The advection term transports contaminants along the prescribed airflow field, whereas the diffusion term represents concentration smoothing resulting from molecular and turbulent mixing. Spatial derivatives are approximated using first-order upwind finite differences for advection and a second-order central finite-difference stencil for diffusion, while temporal integration is performed using an explicit forward Euler scheme.

Unlike conventional finite-volume CFD solvers that iteratively solve coupled momentum and pressure equations over unstructured meshes or cells, the proposed framework assumes that airflow fields are either generated or imported beforehand and focuses on efficiently solving contaminant transport on structured voxel grids. The regular voxel topology enables contiguous memory layouts and predictable neighborhood access patterns, improving memory locality and facilitating efficient GPU-parallel stencil computation. Consequently, each voxel update depends only on local neighborhood information, eliminating the need for global sparse matrix assembly or iterative linear solvers and enabling embarrassingly parallel GPU execution. The computational workflow is summarized in Algorithm 1. The current implementation leverages Python Taichi fields under a data-oriented programming model to organize voxel attributes directly in GPU memory. Structured voxel indices are mapped into contiguous memory layouts to enable efficient neighboring voxel access and scalable stencil-based computation. This modular GPU architecture further supports future integration with CFD-derived airflow fields, AI surrogate models, sparse voxel activation, interactive-scale digital twins, and sensor-driven environmental simulations.

$$\nabla^2 C \approx \frac{C_{i+1,j,k} + C_{i-1,j,k} + C_{i,j+1,k} + C_{i,j-1,k} + C_{i,j,k+1} + C_{i,j,k-1} - 6C_{i,j,k}}{\Delta x^2} \tag{3}$$

where $C_{i,j,k}$ denotes the contaminant concentration at voxel (i, j, k), $C_{i\pm1,j,k}$, $C_{i,j\pm1,k}$, and $C_{i,j,k\pm1}$ represent the concentrations of the six face-connected neighboring voxels, and Δx is the voxel size. This six-neighbor finite-difference stencil provides a second-order

approximation of the Laplacian operator, enabling efficient local diffusion updates while naturally supporting massively parallel GPU execution.

Algorithm 1 GPU-parallel voxel-based gas and aerosol transport update

Require: Voxel grid G, air mask A, species set $\mathcal{S}$, concentration field C, airflow fields U, V, W, timestep Δt, voxel size Δx
Ensure: Updated concentration field $C^{t+\Delta t}$
for all species $s \in \mathcal{S}$ **in parallel do**
  for all voxels $(i, j, k) \in G$ **in parallel do**
    if (i, j, k) is an air voxel **then**
      Read current concentration $C_0 = C_s(i, j, k)$
      Read airflow velocity $\mathbf{u} = (U, V, W)$
      if species s is aerosol **then**
        Adjust vertical velocity using settling velocity: $W \leftarrow W - v_{\text{settle},s}$
      end if
      Retrieve neighboring concentrations using no-flux wall treatment
      Compute advection term using first-order upwind differences
      Compute diffusion term using six-neighbor Laplacian stencil
      Compute source term $S_s(i, j, k)$
      Compute sink rate:

$$\lambda_s = \lambda_{\text{vent},s} + \lambda_{\text{react},s} + \lambda_{\text{dep},s}(i, j, k)$$

      Update concentration:

$$C_s^{t+\Delta t}(i, j, k) = C_0 + \Delta t(Adv_s + Diff_s + S_s - \lambda_s C_0)$$

      Enforce non-negative concentration constraint
    else
      Set $C_s^{t+\Delta t}(i, j, k) = 0$
    end if
  end for
end for
Apply buffer swap: $C \leftarrow C^{t+\Delta t}$

Figure 2 summarizes the design rationale of the proposed GPU implementation. The regular voxel topology transforms contaminant transport into a localized stencil computation in which each voxel update depends only on neighboring concentrations and prescribed airflow fields. This locality minimizes memory indirection, enables contiguous data layouts, and allows thousands of voxel updates to be executed simultaneously by GPU threads. Consequently, the framework achieves high computational throughput while remaining flexible enough to incorporate different airflow generation models and transport formulations through its modular architecture.

3.2.6. Numerical Stability and Time-Step Selection

The proposed framework employs an explicit finite-difference discretization of the voxel-based advection–diffusion equation. Consequently, the simulation timestep must account for both advective and diffusive stability constraints. Unless otherwise specified, a fixed timestep of $\Delta t = 0.02$ s was adopted in the demonstration scenarios. Smaller timesteps were used where required by the corresponding spatial resolution and transport conditions.

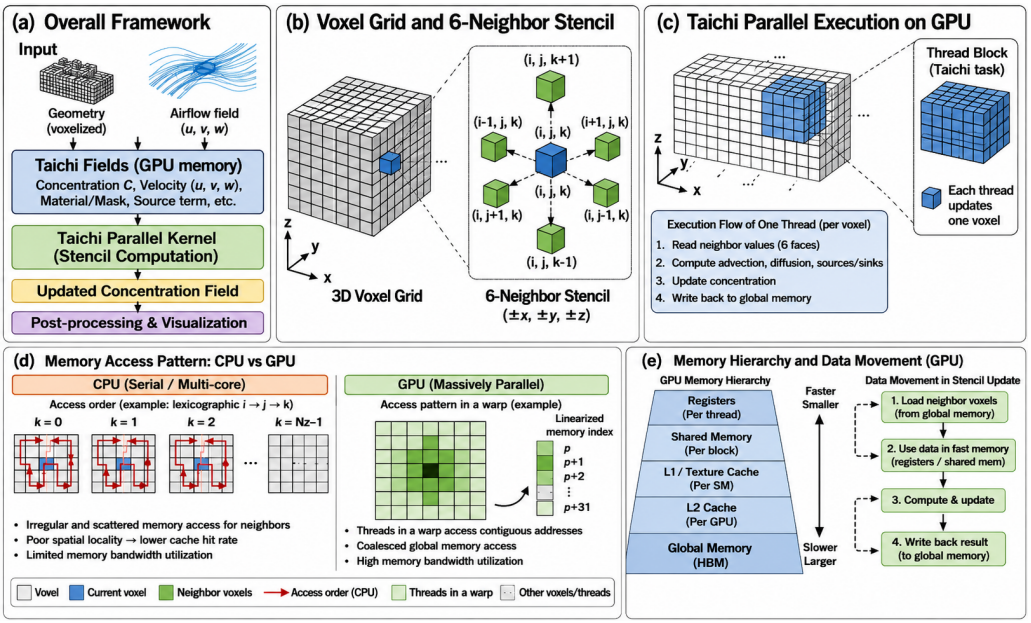


Figure 2. Schematic of the Taichi-based GPU-parallel stencil framework for voxel-based contaminant transport simulation. (**a**) Overall simulation workflow. (**b**) Structured voxel grid and six-neighbor stencil. (**c**) GPU-parallel per-voxel computation. (**d**) CPU and GPU memory access patterns. (**e**) GPU memory hierarchy and data movement during stencil computation.

For the explicit first-order upwind discretization of the advection term, numerical stability is constrained by the Courant–Friedrichs–Lewy (CFL) condition. For the three-dimensional formulation, the combined directional Courant number can be expressed as

$$Co = \Delta t \left(\frac{|u|_{\max}}{\Delta x} + \frac{|v|_{\max}}{\Delta y} + \frac{|w|_{\max}}{\Delta z} \right), \tag{4}$$

where $|u|_{\max}$, $|v|_{\max}$, and $|w|_{\max}$ denote the maximum absolute velocity components in the three coordinate directions, and Δx, Δy, and Δz denote the corresponding voxel spacings. The timestep is selected such that the adopted explicit upwind scheme satisfies the corresponding CFL constraint.

For the explicit three-dimensional diffusion formulation, the stability constraint is

$$D_{\text{eff}} \Delta t \left(\frac{1}{\Delta x^2} + \frac{1}{\Delta y^2} + \frac{1}{\Delta z^2} \right) \leq \frac{1}{2}, \tag{5}$$

where D_{eff} denotes the effective diffusion coefficient, including molecular and, where applicable, turbulent contributions. For the cubic voxel discretization adopted in the present framework, where $\Delta x = \Delta y = \Delta z = \Delta$, the condition reduces to

$$Fo = \frac{D_{\text{eff}} \Delta t}{\Delta^2} \leq \frac{1}{6}. \tag{6}$$

For example, the urban-scale dispersion scenario employs a maximum prescribed airflow velocity of approximately 10 m s^{-1}, a voxel spacing of 0.8 m, and a timestep of 0.02 s. Considering an individual velocity component of 10 m s^{-1} gives a directional Courant number of

$$Co_x = \frac{10 \times 0.02}{0.8} = 0.25.$$

The indoor demonstration scenarios employ lower characteristic airflow velocities of approximately 1.5 m s^{-1} with a finer voxel resolution of 0.2 m, corresponding to a direc-

tional Courant number of approximately 0.15 for a velocity component of this magnitude. In practice, timestep selection considers the velocity components and diffusion coefficients associated with each simulation configuration.

The timestep adopted in each scenario was therefore selected conservatively with consideration of the corresponding advective and diffusive stability constraints. Nevertheless, numerical stability is also influenced by the combined transport formulation, source and sink terms, and boundary treatment. Moreover, satisfying these stability constraints does not eliminate numerical diffusion associated with the first-order upwind discretization, particularly at coarse voxel resolutions or in regions with strong concentration gradients. The present framework is therefore intended as a computationally lightweight approximation of contaminant transport rather than a replacement for high-fidelity CFD solvers employing higher-order discretization and more comprehensive flow physics. Systematic grid-convergence and timestep-sensitivity analyses, together with higher-order transport schemes and adaptive discretization strategies, will be investigated in future work.

4. Exploratory Simulation Demonstrations

This section presents four simulation scenarios to evaluate the capability of the proposed framework for modeling indoor and outdoor contaminant transport under different environmental conditions. The first scenario examines $PM_{2.5}$ aerosol dispersion under varying ventilation conditions. The second compares the transport behaviors of CO and Cl_2 under identical airflow conditions. The third demonstrates urban-scale SF_6 dispersion associated with a hypothetical truck leakage event in downtown Liverpool. The fourth presents an indoor Cl_2 leakage event within a voxelized three-story IFC-derived building model containing approximately 34.5 million active voxels, demonstrating high-resolution indoor contaminant transport and floor-to-floor propagation through complex building geometries.

In addition to qualitative analysis of contaminant propagation and airflow interactions, this section provides a preliminary computational evaluation of the framework. The simulated contaminant concentration is represented as a species mass fraction, providing a consistent scalar representation of contaminant abundance within each voxel. The current study focuses primarily on computational and visual demonstrations, together with a preliminary quantitative comparison against an established CFD benchmark, while more comprehensive validation against experimental measurements, field observations, and additional CFD benchmarks remains future work.

4.1. Scenario 1: Comparative $PM_{2.5}$ Aerosol Transport Under Different Ventilation Conditions

To demonstrate the capability of the proposed voxel-based environmental simulation framework for modeling indoor aerosol transport under different ventilation conditions, we conducted a comparative $PM_{2.5}$ aerosol dispersion experiment using a synthetic two-bedroom indoor floor plan (shown in Figure 3). The indoor environment was voxelized at a spatial resolution of 20 cm, resulting in a structured voxel representation suitable for stencil-based transport simulation and GPU-parallel computation. Two comparative scenarios were designed using the same aerosol source location and source emission rate of 10 g/s in order to isolate the influence of ventilation conditions and airflow dynamics on aerosol transport behavior.

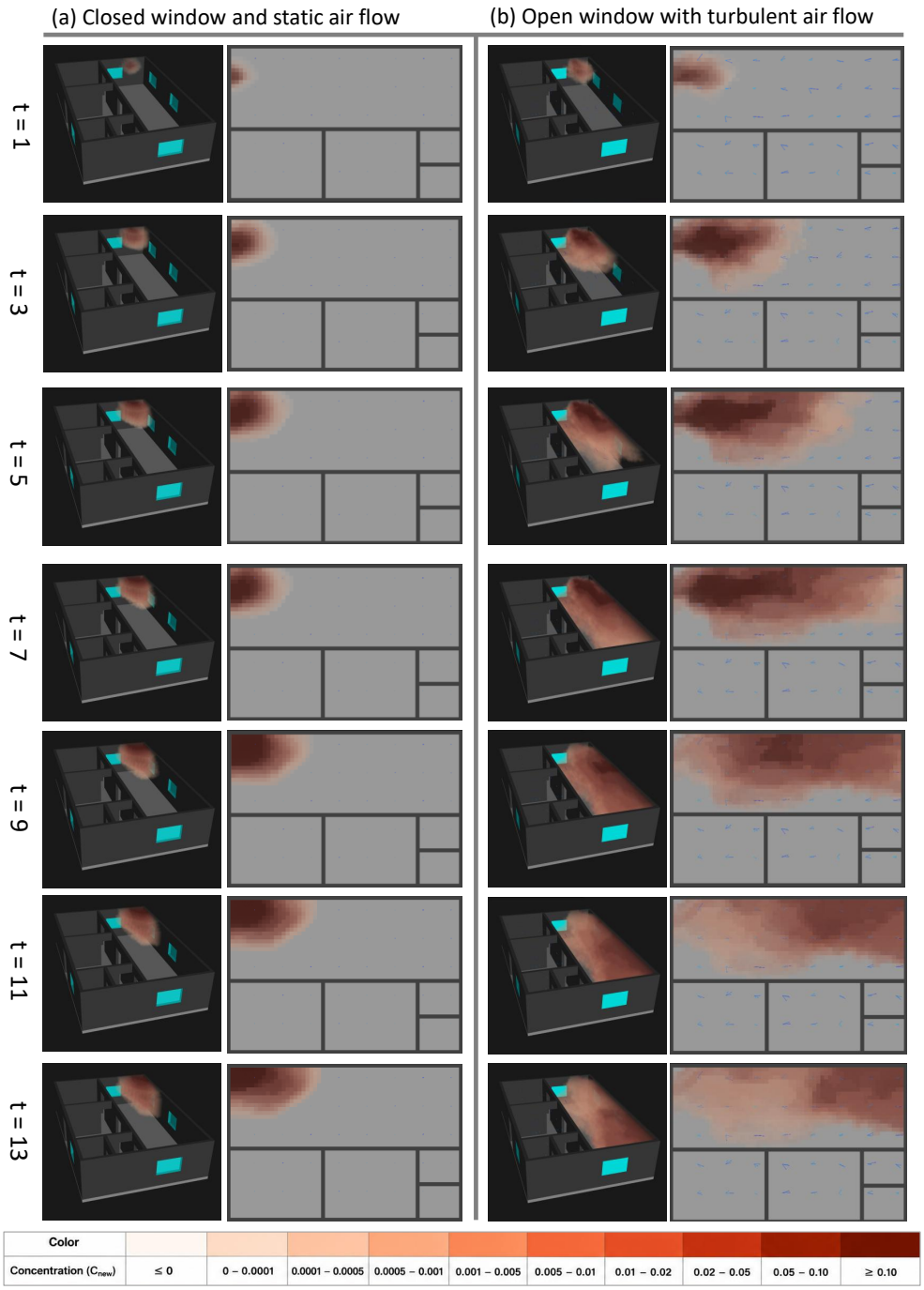


Figure 3. Comparative $PM_{2.5}$ aerosol transport under different ventilation and airflow conditions during the first 13 s. The blue arrows indicate the airflow direction at different heights within the room.

Figure 3a represents a closed indoor environment with closed windows and static airflow conditions. In this configuration, no active ventilation or airflow-driven transport was introduced, resulting in aerosol propagation being primarily governed by localized diffusion and gradual concentration spreading from the source region. Under these conditions, the $PM_{2.5}$ aerosol cloud remained relatively concentrated near the emission source during the early simulation stages and expanded slowly throughout the indoor space over time. The simulation results indicate that the absence of ventilation and airflow mixing leads to persistent aerosol accumulation and limited spatial redistribution, producing relatively localized high-concentration regions within the indoor environment.

In contrast, Figure 3b represents an open-window indoor environment with turbulent airflow conditions. In this scenario, windows were treated as sink voxels with a removal coefficient of $\lambda = 10$ to simulate ventilation-driven aerosol removal. A turbulent airflow field with an average velocity of 1.5 m/s was also introduced to simulate indoor air circulation and mixing. Compared with the closed-environment scenario, the aerosol plume in Figure 3b spread more rapidly across the indoor space and into adjacent rooms due to airflow-driven transport and turbulent mixing. Meanwhile, the ventilation effect at the windows gradually reduced aerosol accumulation by removing airborne particles from the indoor environment.

The comparative results demonstrate that ventilation configuration and airflow dynamics strongly influence aerosol transport behavior within indoor environments. While the closed-environment scenario produced localized aerosol accumulation and slower diffusion-dominated spreading, the turbulent ventilation scenario generated more dynamic transport patterns characterized by rapid mixing, broader spatial propagation, and increased aerosol removal through ventilation sinks. These experiments illustrate the ability of the proposed framework to simulate time-evolving aerosol transport processes under different indoor environmental conditions using configurable airflow fields, material-dependent sink mechanisms, and structured voxel-based transport computation.

4.2. Scenario 2: Comparative Transport Behaviors of CO and Cl_2 Under Identical Airflow Conditions

This scenario investigates the comparative indoor transport behaviors of carbon monoxide (CO) and chlorine gas (Cl_2) within an identical voxelized five-bedroom indoor environment under the same prescribed airflow and ventilation conditions. The synthetic indoor floorplan was configured with open-window ventilation, where window voxels were modeled as sink regions with a material removal coefficient of $\lambda = 10$ to represent ventilation-driven contaminant removal. A turbulent airflow field with a mean airflow velocity of 1.5 m/s was applied throughout the indoor environment to represent indoor air circulation and mixing.

Figure 4 presents the temporal evolution of the simulated CO and Cl_2 plumes at multiple timestamps. Although both species were released under the same environmental and airflow conditions, the simulations produced different spatial transport patterns as a result of the species-specific transport parameters prescribed in the model. CO exhibited broader and more diffuse propagation through the connected rooms and corridors, whereas the simulated Cl_2 plume remained comparatively more spatially concentrated and exhibited stronger localized accumulation.

At $t = 12$ s, the difference between the simulated plume structures is particularly apparent. The CO plume occupies a larger spatial extent and exhibits a more diffuse concentration distribution across the connected indoor spaces. In contrast, the Cl_2 plume retains a more compact spatial structure, with higher localized concentrations and sharper concentration gradients along the primary airflow-driven transport pathway. These differences arise from the species-specific transport parameters adopted in the present simulations and illustrate how the framework can represent different parameterized contaminant-transport behaviors under an otherwise identical prescribed airflow field.

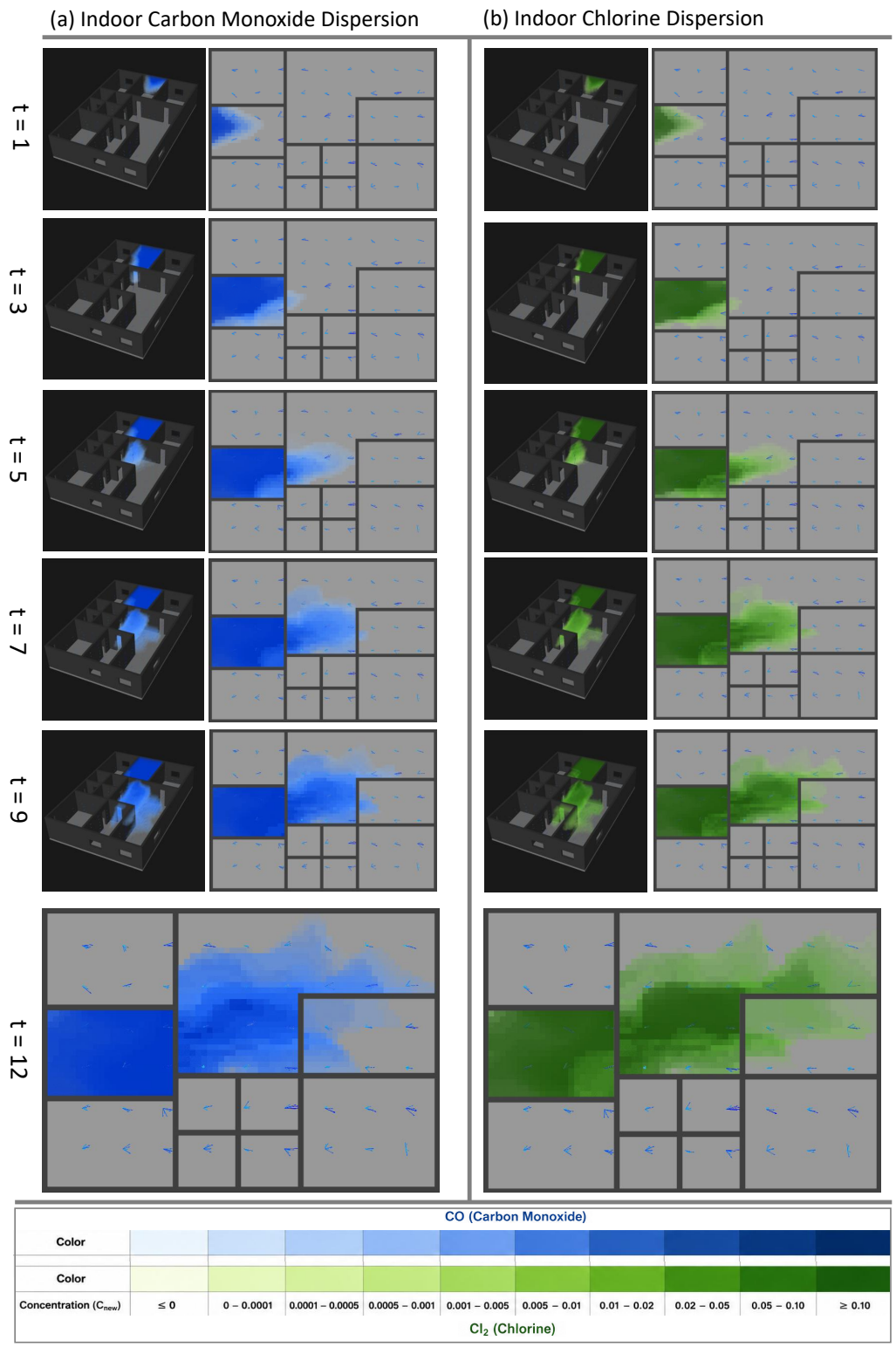


Figure 4. Comparative voxel-based simulation of indoor CO and Cl_2 transport under identical prescribed airflow conditions. The simulations exhibit broader spatial spreading of CO and a more spatially concentrated Cl_2 plume under the species-specific transport parameters adopted in the present framework.

Importantly, the present framework does not explicitly resolve density-driven buoyancy or the feedback of species density on the airflow field. Therefore, the differences observed between the CO and Cl_2 simulations should not be interpreted as a direct numerical reproduction of the physical buoyancy effects associated with lighter- or heavier-than-air

gases. Instead, this scenario provides an exploratory comparison of species-dependent transport behavior arising from the configurable transport properties implemented in the current framework. Explicit coupling of species density, buoyancy, thermal effects, and airflow dynamics will be investigated in future development.

Overall, this scenario demonstrates the ability of the voxel-based framework to represent contrasting species-dependent transport patterns through configurable transport parameters within the same voxelized environment and prescribed airflow field. The comparison is intended as an exploratory demonstration of this capability rather than a quantitative reproduction of density- or buoyancy-driven differences between CO and Cl_2. Incorporating explicit buoyancy and density–flow coupling would enable more physically complete investigation of such differences in future work.

4.3. Scenario 3: Urban-Scale SF_6 Dispersion Associated with a Hypothetical Truck Leakage Event in Downtown Liverpool

This scenario demonstrates a large-scale urban gaseous dispersion simulation involving approximately 13.9 million active voxels within a voxelized representation of downtown Liverpool, Sydney. The experiment models a hypothetical sulfur hexafluoride (SF_6) leakage event originating from a truck positioned within a dense urban street environment. The simulation was conducted using the proposed GPU-accelerated voxel framework under turbulent urban airflow conditions to evaluate its capability for large-scale environmental transport modeling within complex three-dimensional urban geometries. The urban voxel environment was derived from high-resolution LiDAR-based voxel datasets generated using the VoxelMates platform. The simulated domain represents a dense suburban region containing buildings, roads, and vegetation structures at sub-meter voxel resolution. A turbulent airflow field was applied using a synthetic turbulent-uniform wind model with a mean wind speed of 10 m/s, directional flow toward the northwest, turbulence intensity of 0.6, and enhanced vertical circulation to emulate highly dynamic urban airflow interactions.

Figure 5 illustrates the temporal evolution of the simulated SF_6 plume from $t = 1$ to $t = 6$ s. During the early stages, the gaseous plume remained relatively localized near the truck leakage source. As the simulation progressed, the plume expanded rapidly along urban street corridors and around surrounding buildings under strong turbulent advection. The results demonstrate clear interactions between the plume and urban morphology, including directional channeling effects, obstruction by buildings, and vertically expanding turbulent dispersion patterns. At later timestamps, the plume occupied a substantially larger spatial extent, exhibiting complex volumetric propagation behavior across the urban environment.

The experiment demonstrates the capability of the proposed voxel-based framework to support urban-scale gaseous transport simulations involving tens of millions of voxels while preserving explicit three-dimensional urban topology and airflow-driven transport dynamics. The scenario further highlights the potential of the framework for future applications in urban digital twins, environmental hazard assessment, emergency response simulation, and large-scale atmospheric transport modeling.

4.4. Scenario 4: Indoor Chlorine Gas Dispersion Associated with a Hypothetical Container Leakage Event in a Multi-Story Building

This scenario demonstrates a large-scale indoor hazardous gas dispersion simulation within a voxelized three-story building derived from an Industry Foundation Classes (IFC) model. The experiment models a hypothetical Cl_2 release resulting from the catastrophic rupture of a storage container located on the second floor of the building. The indoor environment was voxelized at a spatial resolution of 15 cm, resulting in a voxel domain of $582 \times 382 \times 155$ cells containing approximately 34.5 million active voxels representing

structural elements and interior air spaces. A synthetic airflow field was introduced to represent ventilation and indoor air circulation, enabling contaminant transport between connected spaces and vertical movement through stairwells. The chlorine source was assigned a constant emission rate of 10 kg/s. The complete simulation, including transport calculations across the entire voxel domain, was executed on a single GPU workstation with an average runtime of approximately 546 s.

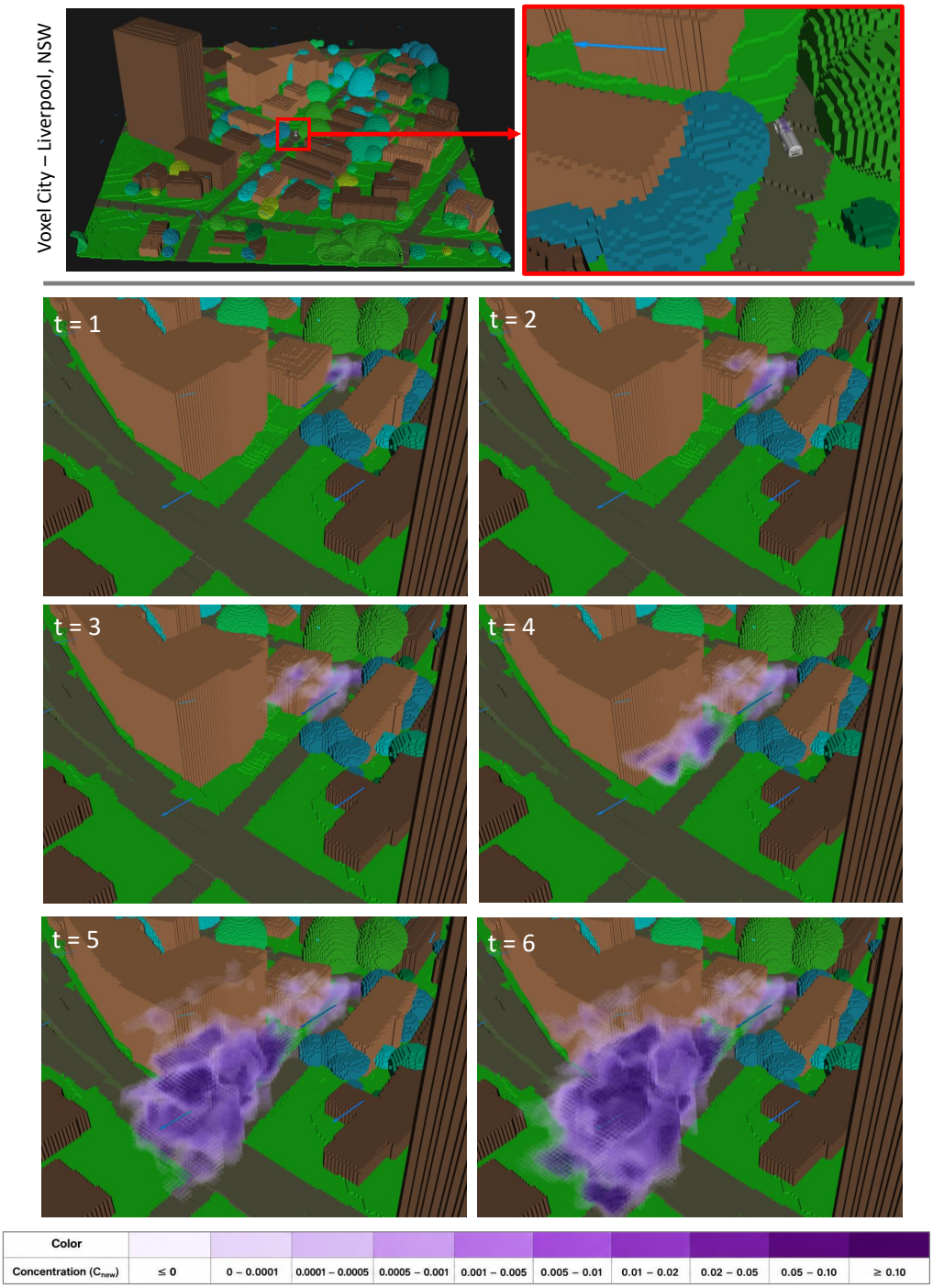


Figure 5. Temporal voxel-based simulation of urban-scale (SF_6) plume propagation within a synthetic voxelized representation of Liverpool, NSW, demonstrating airflow-driven dispersion and volumetric plume expansion through complex urban geometry over time.

Figure 6 illustrates the temporal evolution of the chlorine plume following the release event. Here, T denotes simulation time in milliseconds (ms), and only the first 2500 ms

(2.5 s) are shown to highlight the early-stage dispersion dynamics. At $T = 500$ and $T = 900$ ms, the plume remained concentrated near the source location on the second floor. As the simulation progressed ($T = 1300$ and $T = 1700$ ms), airflow-driven advection and diffusion transported the contaminant throughout adjacent rooms and corridors while gradually increasing its spatial extent. The plume subsequently migrated through the central staircase system, creating a vertical transport pathway between floors.

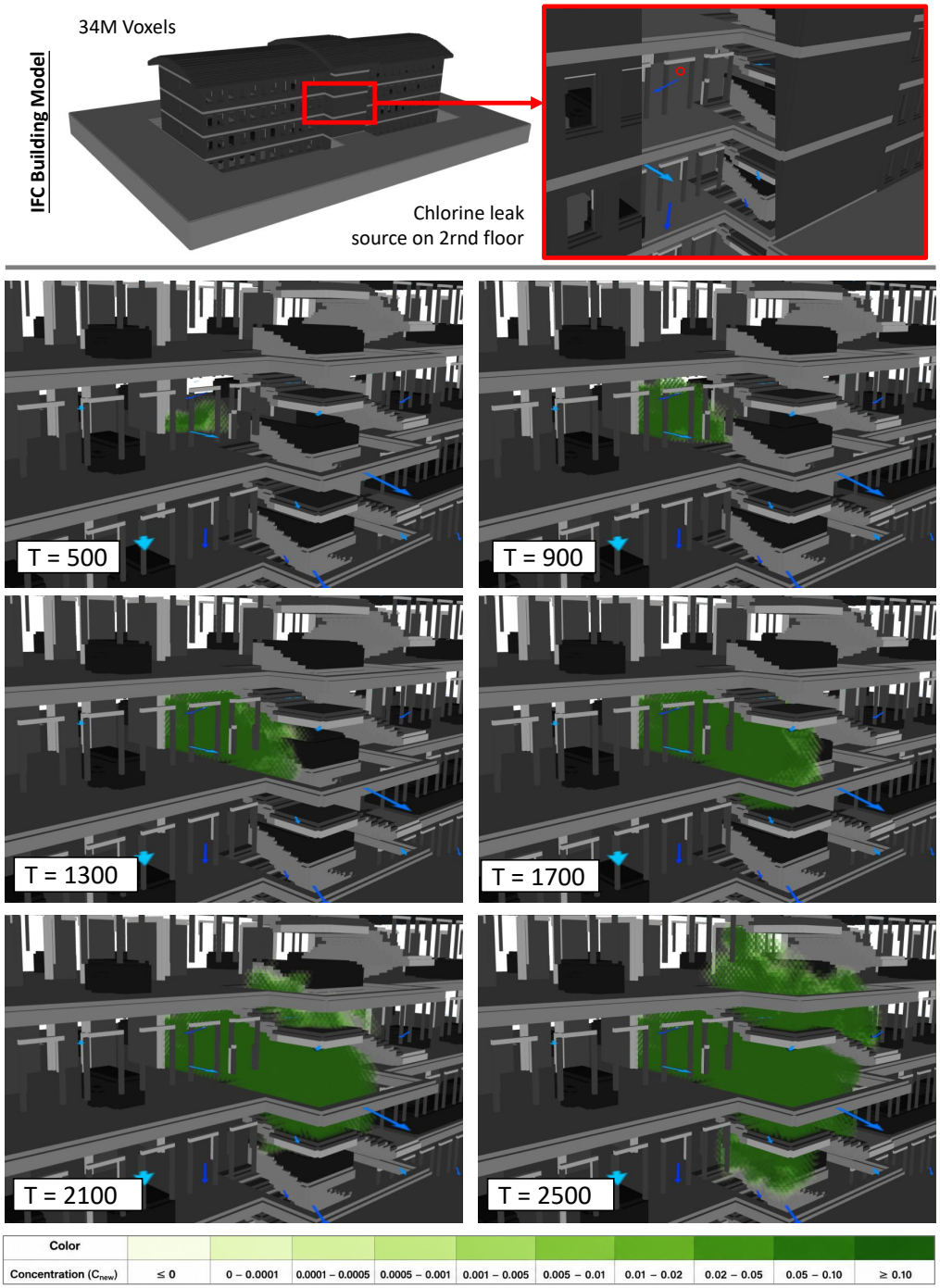


Figure 6. Simulation Simulation of a chlorine gas (Cl_2) leak in a three-story IFC-derived building model containing approximately 34.5 million active voxels. The plume spreads through rooms and stairwells under airflow-driven transport conditions. The blue/cyan arrows indicate the prescribed airflow direction. The red box and associated callout identify and provide an enlarged view of the chlorine release region on the second floor, while the red circle indicates the location of the gas leak source.

By $T = 2100$ and $T = 2500$ ms, substantial contaminant accumulation was observed throughout the second floor, accompanied by significant upward and downward propagation through the stairwell openings. Within approximately 2.5 s, the chlorine plume had spread from the source floor to both the first and third floors, illustrating the rapid transport of airborne contaminants through interconnected indoor spaces. The results highlight the influence of building topology on dispersion processes, including room confinement, corridor channeling, and floor-to-floor migration through vertical circulation pathways. This scenario demonstrates the ability of the proposed framework to perform high-resolution indoor contaminant transport simulations within complex IFC-derived building environments and highlights its potential applications in building digital twins, indoor air quality assessment, hazardous material release analysis, and emergency response planning.

4.5. Scenario Setup and Configuration Summary

To improve the reproducibility of the experimental evaluation, Table 1 summarizes the geometric domains and voxel discretization adopted in the four demonstration scenarios. The accompanying voxelized datasets are also provided as Supplementary Materials in Apache Parquet format to facilitate independent verification and reuse. Scenarios 1 and 2 represent indoor residential environments consisting of two-bedroom and five-bedroom floor plans, respectively. Both scenarios employ a uniform voxel resolution of 0.20 m and are used to demonstrate indoor gas and aerosol dispersion under parameterized airflow conditions. Scenario 3 represents an urban-scale outdoor environment covering approximately $272.6 \times 367.5 \times 104.8$ m and containing approximately 14.0 million active voxels. Scenario 4 consists of a three-story IFC building model with dimensions of $87.15 \times 57.15 \times 23.25$ m and approximately 34.1 million active voxels, demonstrating the scalability of the proposed framework for large three-dimensional built environments.

Across all scenarios, the proposed framework represents the simulation domain using structured Cartesian voxels, allowing the same GPU-parallel stencil-based transport solver to be applied regardless of the underlying environment. Airflow fields may be generated using the built-in parameterized airflow models or imported from external sources, as described in Section 3.2.2, while contaminant transport is solved using the unified voxel-based advection–diffusion framework described in Section 3.2.5. This modular design enables the same computational architecture to support indoor, outdoor, and other application domains by replacing the airflow generation component while preserving the voxel-based transport formulation. The voxelized datasets corresponding to the four experimental scenarios are provided in Apache Parquet format as Supplementary Materials. Each dataset contains voxel indices, spatial coordinates, material classifications, and boundary attributes required to reconstruct the simulation domains, thereby facilitating reproducibility and future benchmarking of voxel-based environmental simulation methods.

Table 1. Summary of the geometric domains and voxel discretization used in the four demonstration scenarios.

Parameter	S1	S2	S3	S4
Environment	2-Bed	5-Bed	Liverpool	IFC
Domain (m)	$12 \times 8 \times 2.8$	$14 \times 10 \times 2.8$	$272.6 \times 367.5 \times 104.8$	$87.2 \times 57.2 \times 23.3$
Resolution (m)	0.20	0.20	0.80	0.15
Grid	$60 \times 40 \times 14$	$70 \times 50 \times 14$	$336 \times 368 \times 131$	$581 \times 381 \times 155$
Active voxels	33,600	49,000	13.98 M	34.09 M

To further facilitate reproducibility, Table 2 summarizes the principal simulation configurations adopted in the four demonstration scenarios, including the contaminant species, source locations, equivalent source strengths, and airflow configurations. Unless other-

wise specified, all scenarios employed the same turbulent-uniform airflow model with a turbulence intensity of 0.6, an eddy size of 2.0 m, a fixed random seed of 123, and a simulation time step of 0.02 s. The vertical turbulence strength was set to 0.5 for the indoor residential scenarios (Scenarios 1–2) and 1.0 for the large-scale urban and building scenarios (Scenarios 3–4). All simulations were continued until the contaminant concentration field converged to a steady-state solution.

Table 2. Summary of the source and airflow configurations used in the four demonstration scenarios.

Parameter	S1	S2	S3	S4
Species	$PM_{2.5}$	Cl_2/CO_2	SF_6	Cl_2
Source voxel	$(1, 30, 10)$	$(1, 26, 11)$	$6@(170, 175, 34)$	$(300, 200, 66)$
Source strength (m^3/s)	0.40	0.80	1.0 *	0.169
Wind speed (m/s)	1.5	1.5	10	8
Wind direction	$(1, 0, 0)$	$(1, 0, 0)$	$(-1, 1, 0)$	$(1, 1, 0)$

* Calculated assuming the specified source strength is applied independently to each of the six source voxels.

4.6. Validation and Verification Against CFD Benchmark Data

A publicly accessible ANSYS Fluent benchmark, Propagation of Car Exhaust Gas in a Ventilated Garage [46], was selected as an external reference for evaluating the proposed voxel-based framework. The benchmark represents three-dimensional exhaust-gas dispersion in a mechanically ventilated enclosed parking garage, where a vehicle continuously releases exhaust, ambient air is induced through an open door, and the resulting air–exhaust mixture is removed through the ventilation system. The resulting non-uniform airflow involves recirculation, dilution, and ventilation-driven contaminant transport, providing a relevant test case for evaluating the spatial transport behavior of the proposed framework.

4.6.1. Benchmark Scenario Selection

The reference CFD case was selected based on its suitability for model comparison and relevance to the application scope of the proposed framework. As this study focuses on three-dimensional contaminant transport in voxelized built environments, the benchmark should represent non-trivial airflow-driven dispersion while providing sufficient information to reconstruct the domain and boundary conditions. Public access to the original CFD files and technical documentation was also considered important for reproducible comparison. Based on these requirements, the ANSYS Fluent garage benchmark was selected according to the following criteria:

- Public accessibility and reproducibility: It was the first suitable three-dimensional CFD benchmark identified for this study for which the Fluent mesh, case, and data files were publicly accessible online together with documented reference results. This enables the reference CFD solution to be independently reconstructed and examined rather than relying solely on published figures.
- Relevance to the application scope: Ventilation-driven contaminant dispersion in an enclosed parking garage is closely aligned with the indoor and built-environment applications considered in this study, including gas transport, ventilation, contaminant removal, and indoor air-quality assessment.
- Non-trivial three-dimensional transport behavior: The benchmark involves ventilation-induced circulation, fresh-air entrainment, contaminant dilution, and recirculation within the garage, providing a more representative evaluation case than a simplified uniform-flow or idealized advection configuration.
- Availability of reference data and documentation: The benchmark provides detailed video tutorials and technical documentation describing the CFD setup, airflow configu-

ration, and exhaust-gas mass-fraction distribution, together with accessible simulation files. These resources facilitate reconstruction of the benchmark and comparison of the spatial plume structure and dominant transport pathways predicted by the two computational approaches.

- Suitability for controlled model comparison: The accessible CFD geometry, boundary configuration, and solution data enable the benchmark configuration to be systematically reconstructed within the voxel environment, reducing uncertainties associated with independently specified geometries, source locations, ventilation configurations, or airflow conditions.

The ANSYS benchmark was used for validation rather than the exploratory demonstration scenarios presented in Section 4, as those scenarios were designed primarily to demonstrate the functionality and applicability of the proposed framework across different environmental configurations. Several scenarios also involve larger urban-scale domains for which corresponding CFD reference solutions under matched geometries and boundary conditions were not available. In contrast, the independently developed ANSYS benchmark provides an accessible external CFD reference that enables a controlled and systematic comparison with the voxel-based simulation.

4.6.2. CFD Scenario Setup and Voxel Environment Replication

The reference CFD domain contains a continuously operating vehicle exhaust source, an open garage door connecting the enclosed domain to the ambient environment, and two mechanical ventilation shafts. The ventilation system extracts the air–exhaust mixture from the garage, inducing ambient-air inflow through the open door. Because the ventilation outlets and garage opening are spatially separated, the resulting airflow is non-uniform and produces a substantial recirculation region within the garage. The incoming ambient air consequently mixes with and dilutes the vehicle exhaust before the mixture is transported toward and removed through the ventilation outlets.

The ANSYS Fluent model employs the k–ω SST turbulence model together with the energy and species-transport models to represent airflow, thermal transport, and dispersion of the air–exhaust mixture. Gravitational acceleration is specified as 9.81 $\mathrm{m\,s^{-2}}$ in the negative z direction, allowing buoyancy effects associated with the elevated exhaust temperature to be represented. The vehicle exhaust is prescribed as a mass-flow inlet with an inlet temperature of 450 K and an exhaust species mass fraction of 1.0, representing the continuous introduction of exhaust into the garage.

The open garage door is represented by a pressure-outlet boundary condition, with an exhaust species mass fraction of zero specified for backflow. Consequently, ventilation-induced reverse flow through the door introduces uncontaminated ambient air into the computational domain. The two mechanical ventilation shafts are represented as mass-flow outlets that continuously remove the air–exhaust mixture from the garage. The remaining garage surfaces define the enclosed solid boundaries of the computational domain. Together, these boundary conditions generate the circulation, dilution, and contaminant-removal behavior used for comparison with the voxel-based framework.

The reference case was solved in ANSYS Fluent for 500 iterations using the numerical configuration specified in the benchmark. The resulting solution exhibits small-amplitude oscillations in the residuals and monitored quantities and is therefore characterized in the accompanying documentation as nearly steady rather than fully converged to an invariant steady state. Nevertheless, these oscillations are sufficiently small for the benchmark solution to be considered suitable for first-order qualitative analysis. The resulting three-dimensional velocity and exhaust species mass-fraction fields were therefore adopted as the CFD reference for the validation presented in this study.

To ensure consistency between the reference CFD case and its voxel-based replication, the scenario configuration was first verified against the accompanying ANSYS tutorial and technical documentation, including the physical models, boundary conditions, species configuration, and numerical settings. Dedicated Python scripts were then developed to parse the original Fluent `.cas.h5` and `.dat.h5` files and programmatically extract the 3D computational mesh and geometry, boundary-zone information, and the spatial locations and extents of the exhaust source, garage opening, and ventilation outlets. These extracted data were subsequently used to reconstruct the corresponding geometry and boundary configuration within the voxel environment, reducing uncertainties associated with manual reconstruction of the benchmark configuration. The spatial dimensions of the CFD domain and the corresponding voxel discretization and boundary-feature locations used for benchmark replication are summarized in Table 3.

Table 3. Spatial dimensions, voxel discretization, and boundary-feature locations used to replicate the ANSYS Fluent CFD garage benchmark.

Parameter	*x*/*i*	*y*/*j*	*z*/*k*
Physical bounds (m)	10.00–20.10	3.00–18.10	0.00–2.60
Domain dimension (m)	10.10	15.10	2.60
Voxel resolution (m)	0.10	0.10	0.10
Number of voxels	101	151	26
Voxel index range	0–100	0–150	0–25
Exhaust source voxel index	35	54	2
Ventilation outlet 1 voxel indices	60–65	100	17–22
Ventilation outlet 2 voxel indices	60–65	120	17–22
Garage opening voxel indices	1–18	0	0–17

4.6.3. Validation Result Discussion

The ANSYS Fluent benchmark reports the transported exhaust species as a mass fraction, whereas the proposed voxel framework represents contaminant transport using its own scalar concentration formulation. As these quantities are generated using different numerical formulations and are not directly equivalent in absolute magnitude, the validation focuses primarily on the spatial characteristics of the predicted contaminant plume rather than a point-by-point comparison of absolute scalar values. To provide a consistent basis for comparison, each scalar field was independently normalized by its respective maximum value, and plume regions were identified using relative thresholds ranging from 0.1% to 10%. The resulting thresholded fields enable the spatial extent, distribution, and overlap of the contaminant plumes to be evaluated across multiple concentration levels without assuming direct equivalence between the absolute scalar magnitudes predicted by the two models.

A direct time-synchronized comparison was not possible because the reference Fluent dataset represents a nearly steady solution and does not provide a corresponding physical simulation time for the reported concentration field. The ANSYS documentation notes small-amplitude oscillations in the residuals and monitored quantities and considers the resulting field suitable for first-order qualitative analysis. In contrast, the proposed voxel framework evolves the contaminant field explicitly over time. For the present comparison, a numerical timestep of 0.005 s was specified to maintain numerical stability, and the simulation outputs extended to a final recorded step of 65,400, with the evaluated output representing approximately 327 s of simulated contaminant propagation. The comparison therefore focuses on the resulting spatial plume distribution relative to the nearly steady CFD reference field rather than on a time-synchronized transient comparison.

As shown in Figure 7, both simulations predict transport of the contaminant away from the vehicle exhaust source and redistribution through the mechanically ventilated garage. The voxel simulation reproduces the dominant plume trajectory and the broader recirculation-driven transport pattern observed in the CFD reference. In particular, the predicted contaminant distribution follows the ventilation-driven circulation from the source region toward the ventilation outlets, while the region influenced by ambient-air entrainment through the garage opening remains comparatively diluted. These characteristics are consistent with the reference benchmark, in which fresh air entering through the garage door mixes with the exhaust and the resulting mixture circulates within the garage before being removed through the ventilation system.

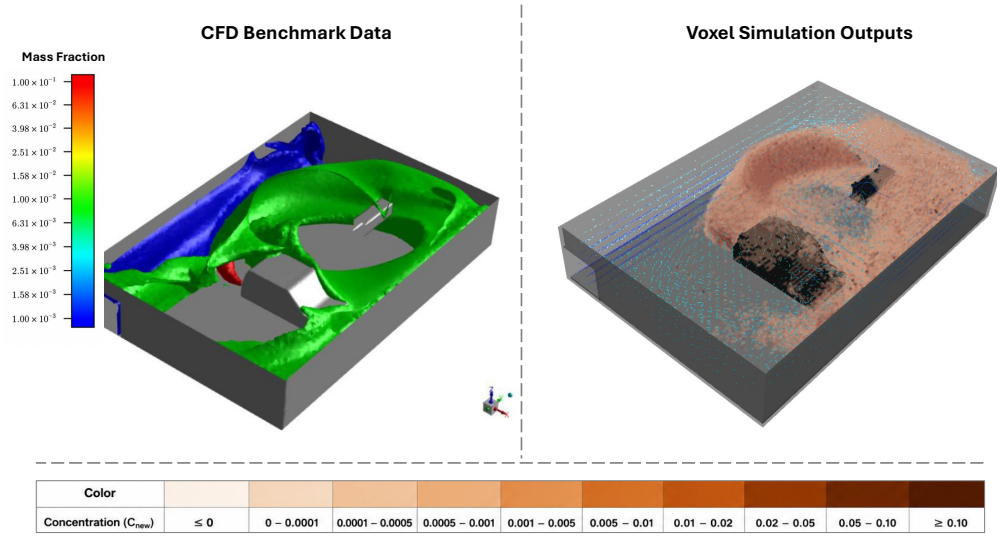


Figure 7. Qualitative comparison of contaminant dispersion predicted by the ANSYS Fluent benchmark (**left**; adapted from [46]) and the proposed voxel-based framework (**right**) for the mechanically ventilated garage. The comparison shows the spatial distribution of the contaminant plume under the matched benchmark configuration. The blue arrows indicate the airflow direction.

To complement the qualitative comparison, spatial agreement between the thresholded CFD and voxel plume regions was quantified using Precision, Recall, F_1 score, Intersection-over-Union (IoU), and Dice coefficient across the selected relative concentration thresholds. The CFD plume was treated as the reference region and the voxel plume as the predicted region. Precision measures the proportion of the predicted plume that correctly overlaps the CFD reference, while Recall measures the proportion of the CFD plume successfully captured by the voxel prediction. The F_1 score is the harmonic mean of Precision and Recall and provides a balanced measure of both. IoU measures the intersection of the CFD and voxel plume regions relative to their union, whereas the Dice coefficient measures twice their intersection relative to the sum of their individual spatial extents. These metrics are widely used to compare binary spatial representations, including image segmentation and geospatial classification, and are therefore suitable for evaluating the spatial correspondence between the three-dimensional plume regions produced by the two models. Results across the evaluated thresholds are summarized in Table 4.

At the 0.1% relative threshold, the comparison achieved a Precision of 0.700, Recall of 0.439, F_1 score of 0.540, IoU of 0.370, and Dice coefficient of 0.540. The Precision of 0.700 indicates that approximately 70% of the plume region predicted by the voxel framework overlaps spatially with the CFD-defined plume at this threshold. The lower Recall of 0.439 indicates that the voxel simulation captures approximately 44% of the total plume region identified in the CFD reference. Taken together, these results indicate stronger agreement in the location of the plume predicted by the voxel framework than in

its complete spatial extent. In other words, the framework captures a substantial portion of the dominant contaminant-transport region but does not reproduce all of the more spatially distributed regions identified by the CFD model. The corresponding F_1 score, IoU, and Dice coefficient further reflect this partial but non-negligible spatial overlap between the two plume predictions.

Table 4. Quantitative comparison between the ANSYS Fluent benchmark and the proposed voxel-based simulation using representative relative concentration thresholds.

Threshold (%)	Precision	Recall	F_1	IoU
0.1	0.700	0.439	**0.540**	**0.370**
0.5	0.658	0.279	0.392	0.243
5.0	0.506	0.250	0.335	0.201

The differences between the two results are consistent with the different levels of physical and numerical representation employed by the models. The Fluent benchmark solves the governing flow equations using the k–ω SST turbulence model together with energy and species transport, whereas the proposed framework uses a simplified voxel-based advection–diffusion formulation driven by the prescribed airflow field. The voxel framework therefore does not independently resolve the same turbulence, buoyancy, and sub-grid mixing processes represented in the CFD calculation. Additional differences may also arise from mapping the original unstructured CFD geometry and solution fields onto the structured 0.10 m voxel grid. These factors can affect plume spreading and the representation of lower-concentration peripheral regions and provide plausible explanations for the lower Recall relative to Precision.

The benchmark comparison should therefore be interpreted as an initial validation of the spatial transport behavior of the proposed framework rather than evidence of CFD-equivalent predictive fidelity. Within this scope, the results provide encouraging evidence that the simplified voxel formulation can reproduce important characteristics of the CFD-predicted contaminant distribution, including the dominant transport direction, ventilation-driven redistribution, and substantial spatial overlap of the plume. Further work can improve the predictive capability of the voxel simulator through refinement of its transport formulations, representation of turbulence and sub-voxel mixing, boundary-condition treatment, and coupling with higher-fidelity airflow models. Additional validation against CFD benchmarks and experimental gas-dispersion measurements across different geometries, ventilation configurations, airflow regimes, and contaminant-release conditions will also be necessary to systematically evaluate and guide these improvements.

4.7. Computational Evaluation

To evaluate the computational performance and practical deployability of the proposed framework, experiments were conducted on a commodity laptop representative of computing platforms that may be available in engineering practice and emergency response applications. The test platform was equipped with an NVIDIA RTX 500 Ada Generation Laptop GPU (4.29 GB VRAM, approximately 3.40 GB available), 32 GB system RAM, and an Intel® Core™ Ultra 7 165H processor running Windows 11 Enterprise (64-bit). Compared with high-performance computing (HPC) platforms, this hardware configuration represents a substantially more resource-constrained computing environment for large-scale voxel-based environmental simulation. Table 5 summarizes the simulation runtime and active voxel count for the four demonstration scenarios, while Figure 8 illustrates the relationship between runtime and problem size. The residential indoor scenarios (Scenarios 1–2), containing 33,600 and 49,000 active voxels, completed 30-min physical

transport simulations in 55 s and 63 s, respectively. The larger outdoor and building-scale scenarios (Scenarios 3–4), containing approximately 13.98 million and 34.09 million active voxels, completed the same 30-min physical simulations in 365 s and 546 s, respectively.

Despite an increase of approximately three orders of magnitude in active voxel count, all four simulations were completed within approximately 9 min on a single consumer-grade GPU. These results demonstrate the computational efficiency and scalability of the proposed GPU-parallel voxel framework, enabling interactive three-dimensional contaminant transport simulation across environments ranging from residential buildings to large urban and complex building models while preserving explicit airflow-driven transport behavior.

Table 5. Simulation runtime and active voxel count for the four demonstration scenarios.

Scenario	Runtime (s)	Active Voxels	Active Voxels (Million)
S1	55	33,600	0.03
S2	63	49,000	0.05
S3	365	13,984,871	13.98
S4	546	34,091,280	34.09

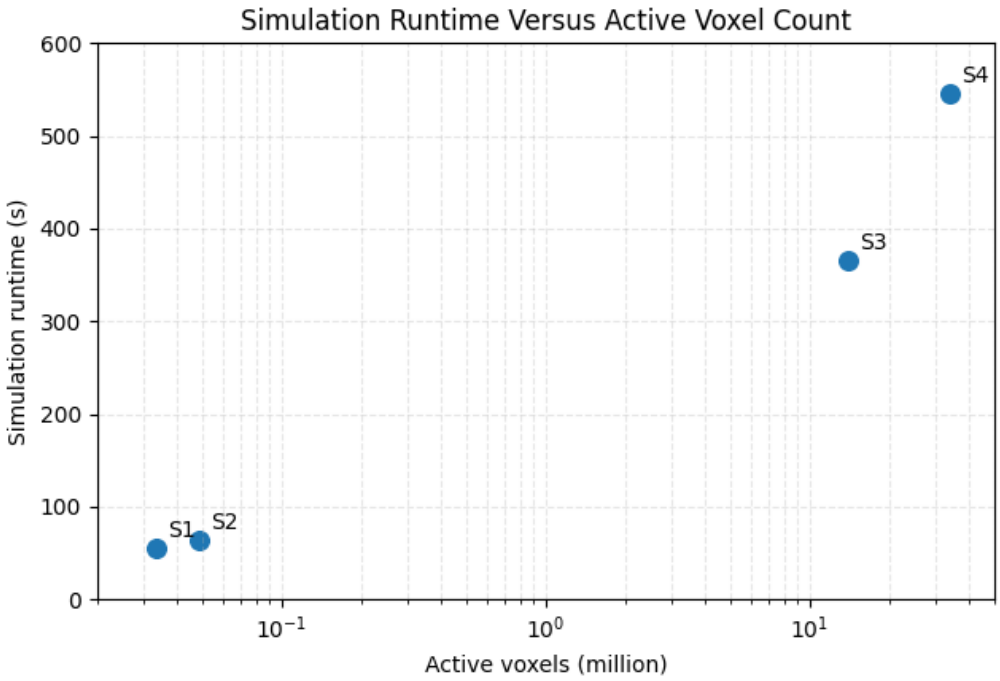


Figure 8. Simulation runtime versus active voxel count for the four demonstration scenarios. The *x*-axis is shown on a logarithmic scale because the active voxel count spans approximately three orders of magnitude. All simulations were performed on a single consumer-grade GPU and continued until convergence to a steady-state solution.

4.8. Current Challenges and Future Work

Although the current prototype demonstrates promising computational efficiency, scalability, and preliminary validation against a benchmark CFD scenario, several important challenges remain.

- First, although the proposed framework has been quantitatively compared with a publicly available ANSYS Fluent benchmark using identical geometry, source conditions, and airflow fields, the current validation remains limited to a single benchmark configuration. Additional validation against real-world experimental datasets and a

broader range of CFD benchmarks is required to comprehensively evaluate the predictive accuracy and generalizability of the framework across different environments, contaminant types, and ventilation conditions.

- Second, large-scale simulation visualization and data management remain challenging due to the substantial size of the generated output datasets. Urban-scale simulations containing tens of millions of active voxels can generate large spatiotemporal datasets, creating bottlenecks in data storage, transfer, loading, and interactive visualization, particularly within browser-based or lightweight visualization environments.
- Third, the current physical formulations remain intentionally lightweight and primarily focus on advection–diffusion transport using prescribed airflow fields. Although the framework supports both imported airflow fields and parameterized voxel-based airflow generators, additional physical processes could be incorporated to improve simulation fidelity. Examples include buoyancy-driven transport, thermal coupling, pressure-driven airflow, humidity effects, chemical reactions, particle deposition, and more sophisticated turbulence representations for gaseous and aerosol transport.

Future work will focus on 3 major directions. First, the proposed framework will be further validated using additional real-world experimental datasets, including NIST benchmark experiments, together with comparative evaluations against established CFD platforms under diverse environmental conditions to further quantify its predictive accuracy and transport fidelity [47]. Second, future developments will investigate scalable visualization and data management strategies, including sparse temporal storage, adaptive compression, progressive streaming, and GPU-accelerated web visualization, to efficiently support interactive exploration of large-scale voxel simulation outputs. Third, the modular voxel-based framework will be extended through the incorporation of additional airflow and transport models, higher-fidelity physical processes, AI surrogate models, and data-driven environmental observations. This extension will also support systematic evaluation of hazardous gases with different density, diffusivity, and buoyancy characteristics, including rapidly dispersing toxic species such as hydrogen cyanide (HCN), thereby providing a broader assessment of the framework across species-specific transport and dispersion regimes. Building on these developments, future research will investigate agentic AI orchestration for automated scenario generation, model selection, simulation steering, and interactive-scale environmental digital twin applications.

4.9. Vision Toward Environmental Decision-Support Infrastructure

Beyond the immediate technical developments outlined above, the proposed framework also provides a longer-term pathway toward environmental digital twins functioning as decision-support infrastructure. In this context, the current gas-dispersion and aerosol-transport simulator should not itself be interpreted as a complete decision-support system. Rather, it provides a computational simulation layer that could be integrated with environmental observations, spatial data, sensor networks, airflow information, human activities, and interactive visualization within a broader digital-twin or cyberinfrastructure environment. The modular voxel representation provides a common spatial structure through which these heterogeneous data and computational components could be integrated and dynamically updated, while the GPU-accelerated simulation capability enables rapid evaluation of evolving environmental hazards under changing conditions. Owing to its modular and programmable architecture, the simulation framework could be incorporated into broader digital-twin applications either as an integrated computational module or as an interoperable simulation service exposed through web-based interfaces and APIs, consis-

tent with the increasingly service-oriented and web-based computational capabilities of modern digital-twin platforms [48,49].

From a decision-support perspective, the framework could contribute to environmental digital twins through three complementary capabilities: understanding what's now," anticipating what's next," and exploring what if." These capabilities align with the broader role of digital twins and decision support systems in supporting situational awareness, predictive analysis, and scenario-based exploration of future and alternative conditions [24,50,51]. The voxel environment can provide a common spatial representation of current 3D environmental conditions by integrating building or urban geometry with available airflow, contaminant, and sensor information. GPU-accelerated simulation can then project the potential evolution of contaminant transport and emerging hazard zones, while alternative simulation scenarios can support what-if" analysis of changes in ventilation, airflow, contaminant sources, openings and barriers, or mitigation measures. For example, the comparative ventilation experiment in Scenario 1 provides a simple demonstration of such scenario-based analysis by evaluating aerosol transport under alternative window and airflow configurations. In a future sensor-informed digital twin, these capabilities could support human-in-the-loop decision-making for hazard assessment, ventilation management, emergency response, and mitigation planning [37]. Longer-term integration with AI agents could further support automated scenario generation, simulation orchestration, comparison of alternative response strategies, and integration of dynamic environmental simulation into 3D world models [24,52,53].

5. Conclusions

This paper presented a GPU-accelerated voxel-based simulation framework for three-dimensional gas dispersion and aerosol transport across indoor and urban environments. The proposed framework integrates voxelized environmental representation, modular airflow modeling, stencil-based advection–diffusion transport simulation, and GPU-parallel computation within a unified Python-based architecture designed for scalable environmental simulation, digital twin applications, and interoperable modeling workflows. Unlike conventional CFD solvers, the framework does not aim to replace high-fidelity airflow simulation, but instead provides a modular computational interface capable of coupling voxel-based contaminant transport with airflow fields generated from CFD, AI surrogate models, urban wind datasets, or lightweight voxel-based airflow generators.

Four demonstration scenarios were presented to evaluate the applicability of the proposed framework across residential indoor, building-scale, and urban environments. the case studies demonstrated $PM_{2.5}$ aerosol transport, parameterized transport of CO, Cl_2, and SF_6, and large-scale contaminant propagation involving up to approximately 34.1 million active voxels. A comparative validation against a publicly available ANSYS Fluent benchmark further demonstrated encouraging agreement in plume morphology and transport pathways under identical geometry, source, and ventilation conditions, while the computational evaluation showed that simulations containing tens of millions of active voxels could be completed within several minutes on a single consumer-grade GPU.

Although the current framework employs simplified transport formulations and a limited benchmark validation, the results demonstrate the feasibility of GPU-parallel voxel-based environmental simulation as an efficient approximation of contaminant transport for interactive environmental analysis. Because airflow generation and contaminant transport are separated, the framework can be adapted to indoor environments, urban areas, and underground mines by replacing the airflow module while preserving the transport solver. Future work will extend validation using additional CFD benchmarks and experimental datasets, incorporate higher-fidelity transport and airflow models, improve large-scale

visualization and data management, and investigate the integration of AI surrogate models and agent-based orchestration with environmental digital twins.

Supplementary Materials: The following supporting information can be downloaded at https://www.mdpi.com/article/10.3390/ijgi15090405/s1, voxelized datasets used in the simulation scenarios in Apache Parquet format.

Author Contributions: Conceptualization, Haowen Xu; methodology, Haowen Xu; software, Haowen Xu; validation, Haowen Xu; formal analysis, Haowen Xu; investigation, Haowen Xu and David Heslop; data curation, Haowen Xu, Sisi Zlatanova, Ben Gorte, Ruiyu Liang and Rabindra Lamsal; visualization, Haowen Xu; writing—original draft preparation, Haowen Xu; writing—review and editing, Sisi Zlatanova, David Heslop, Rabindra Lamsal and Ismet Canbulat; supervision, Sisi Zlatanova; project administration, Sisi Zlatanova. All authors have read and agreed to the published version of the manuscript.

Funding: This research was supported by the 2026 Arts, Design and Architecture (ADA) Faculty Research Grants Scheme at UNSW Sydney (Project ID: PS78645).

Data Availability Statement: The voxelized datasets used in the simulation scenarios are provided as Supplementary Materials in Apache Parquet format.

Conflicts of Interest: The authors declare no conflicts of interest.

References

1. Tran, V.V.; Park, D.; Lee, Y.C. Indoor air pollution, related human diseases, and recent trends in the control and improvement of indoor air quality. *Int. J. Environ. Res. Public Health* **2020**, *17*, 2927. [CrossRef] [PubMed]
2. Mannan, M.; Al-Ghamdi, S.G. Indoor air quality in buildings: A comprehensive review on the factors influencing air pollution in residential and commercial structure. *Int. J. Environ. Res. Public Health* **2021**, *18*, 3276. [CrossRef] [PubMed]
3. Aleksandrov, M.; Zlatanova, S.; Heslop, D.J. Voxelisation algorithms and data structures: A review. *Sensors* **2021**, *21*, 8241. [CrossRef] [PubMed]
4. Xu, H.; Zlatanova, S.; Liang, R.; Canbulat, I. A Modular Light-weight Voxel-Based 3D Wildfire Propagation Simulator in Python Using LiDAR Data, High-Performance Computing (HPC), and Immersive Scientific Visualization. *ISPRS Ann. Photogramm. Remote Sens. Spat. Inf. Sci.* **2026**, *10*, 127–134. [CrossRef]
5. Sadeghi, S.; Aminossadati, S.M.; Leonardi, C. A Critical Review of Critical Factors Influencing Airborne Particle Transmission in Indoor Environments Under Stationary and Dynamic Scenarios. *Arch. Comput. Methods Eng.* **2026** , *33*, 3359–3389. [CrossRef]
6. Rajagopalan, P.; Goodman, N. Improving the indoor air quality of residential buildings during bushfire smoke events. *Climate* **2021**, *9*, 32. [CrossRef]
7. Li, Y.; Leung, M.; Tang, J.; Yang, X.; Chao, C.Y.H.; Lin, J.Z.; Lu, J.; Nielsen, P.V.; Niu, J.; Qian, H.; et al. Role of ventilation in airborne transmission of infectious agents in the built environment—A multidisciplinary systematic review. *Indoor Air* **2007**, *17*, 2–18. [CrossRef] [PubMed]
8. Boje, C.; Guerriero, A.; Kubicki, S.; Rezgui, Y. Towards a semantic Construction Digital Twin: Directions for future research. *Autom. Constr.* **2020**, *114*, 103179. [CrossRef]
9. Hobeika, N.; García-Sánchez, C.; Bluyssen, P.M. Assessing indoor air quality and ventilation to limit aerosol dispersion—Literature review. *Buildings* **2023**, *13*, 742. [CrossRef]
10. Aleksandrov, M.; Zlatanova, S.; Heslop, D.J.; Diakite, A. BIM-based connectivity graph and voxels classification for pedestrian-hazard interaction. *J. Spat. Sci.* **2024**, *69*, 699–719. [CrossRef]
11. Nielsen, P.V. Fifty years of CFD for room air distribution. *Build. Environ.* **2015**, *91*, 78–90. [CrossRef]
12. Chen, Q. Ventilation performance prediction for buildings: A method overview and recent applications. *Build. Environ.* **2009**, *44*, 848–858. [CrossRef]
13. Liu, W.; Jin, M.; Chen, C.; You, R.; Chen, Q. Implementation of a fast fluid dynamics model in OpenFOAM for simulating indoor airflow. *Numer. Heat Transf. Part A Appl.* **2016**, *69*, 748–762. [CrossRef]
14. ANSYS, Inc. *Ansys Fluent Theory Guide*; ANSYS, Inc.: Canonsburg, PA, USA , 2023.
15. McGrattan, K.; Hostikka, S.; McDermott, R.; Floyd, J.; Weinschenk, C.; Overholt, K. *Fire Dynamics Simulator User's Guide*; NIST Special Publication; NIST: Gaithersburg, MD, USA, 2013; Volume 1019, pp. 1–339.
16. Morawska, L.; Tang, J.W.; Bahnfleth, W.; Bluyssen, P.M.; Boerstra, A.; Buonanno, G.; Cao, J.; Dancer, S.; Floto, A.; Franchimon, F.; et al. How can airborne transmission of COVID-19 indoors be minimised? *Environ. Int.* **2020**, *142*, 105832. [CrossRef] [PubMed]

17. Cernei, A.; Thevenet, F.; Bode, F.; Verriele, M.; Nastase, I. Critical Review of Current Validation Methodologies and Future Developments in CFD-Based Indoor Environmental Quality Analysis. *Indoor Air* **2025**, *2025*, 6601284. [CrossRef]
18. Shree, V.; Marwaha, B.M.; Awasthi, P. Assessment of indoor air quality in buildings using CFD: A brief review. *Int. J. Math. Eng. Manag. Sci.* **2019**, *4*, 1154. [CrossRef]
19. Fuller, A.; Fan, Z.; Day, C.; Barlow, C. Digital twin: Enabling technologies, challenges and open research. *IEEE Access* **2020**, *8*, 108952–108971. [CrossRef]
20. Yang, J.; Mu, L.; Grigsby-Toussaint, D. Public perceptions and expectations of urban park environments on children's play: A GIS and text mining analysis on children's activity in Atlanta's parks using social media data. *Environ. Plan. B Urban Anal. City Sci.* **2025**, *52*, 412–429. [CrossRef]
21. Łach, Ł.; Svyetlichnyy, D. Advances in numerical modeling for heat transfer and thermal management: A review of computational approaches and environmental impacts. *Energies* **2025**, *18*, 1302. [CrossRef]
22. Chen, Q.; Zhang, Z.; Zuo, W. Computational fluid dynamics for indoor environment modeling: Past, present and future. In Proceedings of the Proceedings XXV Congresso della Trasmissione del Calore UIT, Trieste, Italy, 18–20 June 2007 .
23. Lu, Y.; Liu, C.; Kevin, I.; Wang, K.; Huang, H.; Xu, X. Digital Twin-driven smart manufacturing: Connotation, reference model, applications and research issues. *Robot. Comput.-Integr. Manuf.* **2020**, *61*, 101837. [CrossRef]
24. Xu, H.; Zlatanova, S.; Li, X.; Wachowicz, M.; Batty, M. Towards fully automated city operations: Integrating agentic AI with urban digital twins. *Comput. Environ. Urban Syst.* **2026**, *128*, 102449. [CrossRef]
25. Ndlovu, Z. Turbulent diffusion and air pollution: A comprehensive review of mechanisms, impacts, and modeling approaches. *World J. Adv. Res. Rev.* **2024**, *23*, 1511–1525. [CrossRef]
26. Fabregat, A.; Pallares, J. Transport and wall surface deposition of airborne particles in enclosed, buoyancy-driven turbulent flows using fully-resolved numerical simulations. *Int. Commun. Heat Mass Transf.* **2022**, *134*, 106048. [CrossRef]
27. Jiang, G.; Wu, M.; Li, H.; Wu, Y. Mechanism of Wind and Buoyancy Driving on Ventilation and Pollutant Transport in an Idealized Urban Street Canyon. *Buildings* **2024**, *14*, 3168. [CrossRef]
28. Lai, A. Particle deposition indoors: A review. *Indoor Air* **2002**, *12*, 211–214. [CrossRef]
29. Pirouz, B.; Palermo, S.A.; Naghib, S.N.; Mazzeo, D.; Turco, M.; Piro, P. The role of HVAC design and windows on the indoor airflow pattern and ACH. *Sustainability* **2021**, *13*, 7931. [CrossRef]
30. Mata, T.M.; Martins, A.A.; Calheiros, C.S.; Villanueva, F.; Alonso-Cuevilla, N.P.; Gabriel, M.F.; Silva, G.V. Indoor air quality: A review of cleaning technologies. *Environments* **2022**, *9*, 118. [CrossRef]
31. Gao, N.; Niu, J. Modeling particle dispersion and deposition in indoor environments. *Atmos. Environ.* **2007**, *41*, 3862–3876. [CrossRef] [PubMed]
32. Pope, S.B. Turbulent flows. *Meas. Sci. Technol.* **2001**, *12*, 2020–2021. [CrossRef]
33. Ashgriz, N.; Mostaghimi, J. An introduction to computational fluid dynamics. In *Fluid Flow Handbook*; McGraw-Hill: New York, NY, USA , 2002; Volume 1, pp. 1–49.
34. Versteeg, H.; Malalasekera, W. Computational fluid dynamics. In *The Finite Volume Method*; Pearson Education: London, UK, 1995; pp. 1–26.
35. Zhai, Z. Application of computational fluid dynamics in building design: Aspects and trends. *Indoor Built Environ.* **2006**, *15*, 305–313. [CrossRef]
36. Ferziger, J.H.; Perić, M.; Street, R.L. *Computational Methods for Fluid Dynamics*; Springer: Berlin/Heidelberg, Germany , 2002; Volume 3.
37. Niloofar, P.; Lazarova-Molnar, S.; Omitaomu, F.; Xu, H.; Li, X. A general framework for human-in-the-loop cognitive digital twins. In *Proceedings of the 2023 Winter Simulation Conference (WSC)*; IEEE: Piscataway, NJ, USA, 2023; pp. 3202–3213.
38. Shao, Y.; Wang, C.; Berres, A.; Yoshioka, J.; Cook, A.; Xu, H. Computer vision-enabled smart traffic monitoring for sustainable transportation management. In *Proceedings of the International Conference on Transportation and Development 2022*; American Society of Civil Engineers: Reston, VA, USA, 2022; pp. 34–45.
39. Xu, H.; Shao, Y.; Chen, J.; Wang, C.; Berres, A. Semi-automatic geographic information system framework for creating photo-realistic digital twin cities to support autonomous driving research. *Transp. Res. Rec.* **2024**, *2678*, 1068–1084. [CrossRef]
40. Xu, H.; Zlatanova, S.; Liang, R.; Canbulat, I. Collaborative Fire Management for Community Wildfire Prevention Using Agentic AI, Simulation, and Mixed-Reality Visualization. *SSRN* **2025**. [CrossRef]
41. Fujiwara, K.; Tsurumi, R.; Kiyono, T.; Fan, Z.; Liang, X.; Lei, B.; Yap, W.; Ito, K.; Biljecki, F. VoxCity: A seamless framework for open geospatial data integration, grid-based semantic 3D city model generation, and urban environment simulation. *arXiv* **2025**, arXiv:2504.13934.
42. Gorte, B.; Zlatanova, S.; Pilouk, M.; Diakite, A.; Barton, J. 3D data integration in the voxel domain. *ISPRS Ann. Photogramm. Remote Sens. Spat. Inf. Sci.* **2024**, *10*, 133–140. [CrossRef]

43. Xu, H.; Berres, A.; Shao, Y.; Wang, C.R.; New, J.R.; Omitaomu, O.A. Toward a smart metaverse city: Immersive realism and 3d visualization of digital twin cities. In *Advances in Scalable and Intelligent Geospatial Analytics*; Taylor & Francis: Abingdon, UK, 2023; pp. 245–257.
44. Nazarian, N.; Lu, J.; Lipson, M.J.; Hart, M.A.; Liu, S.; Krayenhoff, E.S.; Blunn, L.; Martilli, A. UrbanTALES: A large-eddy simulation dataset for urban canopy layer turbulence and parameterization. *Bull. Am. Meteorol. Soc.* **2025**, *106*, E2461–E2478. [CrossRef]
45. Snaiki, R.; Lu, J.; Li, S.; Nazarian, N. A hierarchical deep learning model for predicting pedestrian-level urban winds. *Build. Environ.* **2026**, *245*, 114354. [CrossRef]
46. ANSYS. Simulation Example: Propagation of Car Exhaust Gas in a Ventilated Garage. ANSYS Innovation Space. Available online: https://innovationspace.ansys.com/courses/courses/intro-to-fluid-dynamics/lessons/simulation-example-propagation-of-car-exhaust-gas-in-a-ventilated-garage/ (accessed on 10 August 2026).
47. Pitts, W.M.; Yang, J.; Fernandez, M. *Experimental Characterization of Helium Dispersion in a-Scale Two-Car Residential Garage (NIST TN 1694)*; CreateSpace Independent Publishing Platform: Seattle, WA, USA, 2011.
48. Santhanavanich, T.; Padsala, R.; Coors, V. An OGC API–based framework for scalable and interoperable urban digital twin ecosystems: Insights from the OGC Urban Digital Twins Interoperability Pilot. *Int. Arch. Photogramm. Remote Sens. Spat. Inf. Sci.* **2025**, *48*, 135–140. [CrossRef]
49. Olawade , D.B.; Ijiwade, J.O.; Ojo, A.; Alabi, J.O.; Makanjuola, B.D.; Wada, O.Z. Digital Twin Technology for Environmental Management: Applications, Benefits, and Implementation Challenges. *Environ. Pollut. Manag.* **2026**, *3*, 418–435. [CrossRef]
50. Xu, H.; Berres, A.; Yoginath, S.B.; Sorensen, H.; Nugent, P.J.; Severino, J.; Tennille, S.A.; Moore, A.; Jones, W.; Sanyal, J. Smart mobility in the cloud: Enabling real-time situational awareness and cyber-physical control through a digital twin for traffic. *IEEE Trans. Intell. Transp. Syst.* **2023**, *24*, 3145–3156. [CrossRef]
51. Xu, H.; Windsor, M.; Muste, M.; Demir, I. A web-based decision support system for collaborative mitigation of multiple water-related hazards using serious gaming. *J. Environ. Manag.* **2020**, *255*, 109887. [CrossRef] [PubMed]
52. Xu, H.; Omitaomu, F.; Sabri, S.; Zlatanova, S.; Li, X.; Song, Y. Leveraging Generative AI for Urban Digital Twins: A Scoping Review on the Autonomous Generation of Urban Data, Scenarios, Designs, and 3D City Models for Smart City Advancement. *Urban Inform.* **2024**, *3*, 29. [CrossRef]
53. Zhen, H.; Qiu, X.; Chen, P.; Yang, J.; Yan, X.; Du, Y.; Hong, Y.; Gan, C. 3D-VLA: A 3D Vision-Language-Action Generative World Model. *arXiv* **2024**, arXiv:2403.09631.

Disclaimer/Publisher's Note: The statements, opinions and data contained in all publications are solely those of the individual author(s) and contributor(s) and not of MDPI and/or the editor(s). MDPI and/or the editor(s) disclaim responsibility for any injury to people or property resulting from any ideas, methods, instructions or products referred to in the content.